Pathway-specific responses of isoprene-derived secondary organic aerosol formation to anthropogenic emission reductions in a megacity in eastern China

Huilin Hu[1], Yunyi Liang[2], Ting Li[2], Yongliang She[2], Yao Wang[1,3], Ting Yang[1], Min Zhou[4], Ziyue Li[1], Chenxi Li[1], Huayun Xiao[1], Jianlin Hu[2], Jingyi Li[2,*], Yue Zhao[1,*]

[1]School of Environmental Science and Engineering, Shanghai Jiao Tong University, Shanghai 200240, China

[2]Jiangsu Key Laboratory of Atmospheric Environment Monitoring and Pollution Control, Collaborative Innovation Center of Atmospheric Environment and Equipment Technology, School of Environmental Science and Engineering, Nanjing University of Information Science and Technology, Nanjing 210044, China

[3]Ningbo Ecological and Environmental Monitoring Center, Ningbo 315012, China,

[4]State Environmental Protection Key Laboratory of the Cause and Prevention of Urban Air Pollution Complex, Shanghai Academy of Environmental Sciences, Shanghai 200233, China

Correspondence: Yue Zhao (yuezhao20@sjtu.edu.cn); Jingyi Li (Jingyili@nuist.edu.cn)

ABSTRACT:Isoprene-derived secondary organic aerosol (iSOA) represents a major biogenic source of atmospheric OA ~~and~~, with its formation ~~is profoundly~~ strongly influenced by anthropogenic emissions. However, long-term iSOA measurements in polluted urban regions remain scarce, limit~~ed,~~ ~~hindering the~~ing the understanding of anthropogenic influences on iSOA formation. In this study, field observations of iSOA were conducted in Shanghai, China during summers and winters of 2015, 2019, and 2021, aiming to assess the iSOA response to emission reductions over this period. The particulate iSOA tracers, formed via reactive uptake of isoprene-derived epoxides ~~epoxydiol (IEPOX), a hydroperoxy radical-dominated pathway, and hydroxymethylmethyl-α-lactone (HMML) and/or methacrylic acid epoxide (MAE), a NO_x-dominated pathway,~~ were measured by ~~mass spectrometry~~ gas chromatography-mass spectrometry and high-resolution liquid chromatography-mass spectrometry. After accounting for the measurement uncertainties, ~~B~~both total ~~and IEPOX-derived~~ iSOA and organosulfates (OSs) tracers (including 2-methyltetrol sulfates and 2-methylglyceric acid sulfate) decreased ~~markedly from 2015 to 2021~~annually, while summertime ~~HMML/MAE SOA~~polyol tracers like 2-methyltetrols (2-MTs) and 2-methylglyceric acid (2-MG) ~~did not~~ var~~y~~ied insignificantly despite strong NOx reductions. Declining aerosol reactivity toward ~~IEPOX/HMML/MAE~~isoprene-derived epoxides and reduced atmospheric oxidizing capacity drove the decrease in ~~IEPOX SOA~~ OSs but could not explain the trend of summertime ~~HMML/MAE SOA~~polyols. Simulations ~~of iSOA~~ with the Community Multiscale Air Quality model in 2015 and 2019 captured the decreas~~ing IEPOX SOA trend~~e in total iSOA and OSs,~~and~~ confirm~~ing~~ed a driving role of chemical processes. However, the model failed to replicate relatively stable ~~HMML/MAE SOA~~polyol levels in summer, suggesting additional factors (e.g., ~~the~~ potential unaccounted sources of 2-MTs and methacrolein, the precursor to ~~HMML/MAE~~2-MG) may buffer ~~HMML/MAE SOA~~their variations. These findings ~~demonstrate~~highlight ~~the~~ pathway-specific iSOA responses to emission reductions in a megacity and ~~emphasize~~ the importance of targeted anthropogenic emission reductions for mitigating biogenic SOA formation through regulating ~~regulating~~ atmospheric oxidizing capacity and aerosol reactivity ~~to mitigate biogenic SOA formation in urban environments~~.

1. Introduction

Isoprene (2-methyl-1,3-butadiene, C_5H_8), mainly emitted by terrestrial vegetation, represents the largest source of atmospheric non-methane hydrocarbons, with a global emission flux of 500-750 Tg yr^{-1} (Guenther et al., 2006). Because of its large abundance and high reactivity, the oxidation of isoprene contributes significantly to the formation of secondary organic aerosol (SOA) in the troposphere, estimated to 19.~~2~~ 6 TgC yr^{-1} (Kelly et al., 2018) ~~(Heald et al., 2008)~~. The formation chemistry of isoprene-derived SOA (iSOA) has been extensively studied in laboratory, field, and modelling studies, which have shown that anthropogenic pollutants such as nitrogen oxides (NO_x) and sulfur dioxide (SO_2, the precursor to particulate sulfate) play a crucial role in the formation of iSOA (Shrivastava et al., 2019).

Photooxidation is the dominant fate of isoprene in the atmosphere, during which the C=C bond of isoprene is initially attacked by OH radicals to produce an alkyl radical (Teng et al., 2017), followed by the formation of isoprene hydroxyperoxy radicals ($ISOPO_2$) via oxygen addition (Surratt et al., 2010). The fate of $ISOPO_2$ radicals depends on the environmental conditions. When the NO_x level is sufficiently low (referred to as HO_2-dominated conditions), $ISOPO_2$ would mainly react with HO_2 radicals to form hydroxyhydroperoxides (ISOPOOH) (Paulot et al., 2009). Further OH radical addition to ISOPOOH produces isomeric isoprene epoxydiols (IEPOX, trans-β-IEPOX: cis-β-IEPOX = 0.63:0.37) with a yield of ~70-80% (Paulot et al., 2009; Bates et al., 2014; St. Clair et al., 2016). The gaseous IEPOX can be taken up into aqueous aerosol and undergo acid-catalyzed reactions to form polyols, organosulfates (OSs), and oligomers (Hettiyadura et al., 2019; Lin et al., 2012; Surratt et al., 2010). Several constituents including 2-methyltetrols (2-MTs) and their oligomers, C_5-alkene triols, methyl tetrahydrofurans, and 2-methyltetrol sulfates (2-MT-OS), which were extensively~~abundantly~~ measured in both laboratory-generated and ambient SOA (Xu et al., 2015; Isaacman-Vanwertz et al., 2016; Surratt et al., 2010; Surratt et al., 2007; Worton et al., 2013; Yee et al., 2020), have been employed as molecular tracers of SOA derived from reactive uptake of IEPOX (IEPOX-SOA).

When the NO_x level is high (referred to as NOx-dominated conditions), $ISOPO_2$ would preferentially react with NO, producing unsaturated carbonyls such as methacrolein (MACR) and methyl vinyl ketone (MVK). A large fraction (~~~~~ 45%) of MACR can be further oxidized by OH

75   radicals via aldehydic H-abstraction, followed by oxygen addition to form an acylperoxy radical,

76     $MACRO_2$ (Orlando et al., 1999). Subsequent reaction between $MACRO_2$ and NO_2 yields MPAN, which

77   was proposed to form hydroxymethyl methyl-α-lactone (HMML) or methacrylic acid epoxide (MAE)

78   (Lin et al., 2013b; Nguyen et al., 2015). Both of these two epoxides can undergo heterogeneous acid-

79   catalyzed reactions to form 2-methylglyceric acid (2-MG) as well as its oligoesters and sulfated

80   derivatives (2-methylglyceric acid sulfate, 2-MG-OS), which serve as the molecular tracers of

81   HMML&/MAE-derived SOA (Kjaergaard et al., 2012; Lin et al., 2013b).

82   In addition to altering the fate of RO_2 (including $ISOPO_2$ and $MACRO_2$), NO_x also plays an

83   essential role in regulating atmospheric oxidizing capacity (e.g., the OH level), which governs the

84   photooxidation rate of isoprene in the atmosphere. Compared to NOx that strongly affect the gas-phase

85   oxidation chemistry of isoprene, sulfate aerosol mainly exerts influences on the multiphase chemistry

86   of isoprene-derived epoxides. On one hand, sulfate serves as an important nucleophile in the reactive

87   uptake of isoprene epoxides to form OSs, which competes with the reaction of epoxides with water (Lin

88   et al., 2013b). On the other hand, sulfate can alter the physicochemical properties of particles such as

89   liquid water content (LWC), acidity, and phase state (Zhao et al., 2018; Zhao et al., 2019; Ye et al.,

90   2018), which are the key factors influencing the multiphase reactivity of epoxides and the formation of

91   iSOA.

92   Because of the complexity in the gas-phase and multiphase chemistry leading to iSOA formation,

93   the product distribution of HO_2- versus NO_x-dominated pathways as well as their dependence on

94   different influencing factors (i.e., NOx, sulfate, LWC, and aerosol acidity) varies significantly in

95   different environments. A number of field measurements have found that the formation of IEPOX-SOA

96   tracers was predominated over the HMML&/MAE-SOA tracers, even in some NO_x-rich urban areas

97   (Zhang et al., 2022; Hu et al., 2008; Yee et al., 2020), while a few studies showed that the production

98   of HMML&/MAE-SOA was more prevalent, e.g., in Tianjin, China (Fan et al., 2020) and urban areas

99   of California (Lewandowski et al., 2013). Sulfate was found to be the primary driver of isoprene-derived

100   SOA in rural and urban regions as the iSOA correlated strongly with sulfate while such correlation did

101   not occur with LWC and pH, e.g., in central Amazonia and southeastern U.S (Xu et al., 2015; Yee et al.,

102   2020). It should be noted that significant uncertainties exist in the quantification of iSOA tracers in

103 ambient aerosols due to the lack of authentic standards and/or the presence of measurement artifacts

104 (e.g., matrix effects) (Fu et al., 2012; Wang et al., 2008; Ding et al., 2014; Fu et al., 2016; Fu et al.,

105 2014; Fan et al., 2020; Zhong et al., 2021). ~~Furthermore, previous studies have mainly focused on the~~

106 ~~characterization of the particle-phase abundance of the iSOA tracers~~ (Zhang et al., 2022; Zhang et al.,

107 2019; Kang et al., 2018). ~~Given that the iSOA tracers can actively partition between gas and particle~~

108 ~~phases, considering their particle-phase concentration only may significantly bias our understanding of~~

109 ~~the atmospheric abundance and chemistry of iSOA~~ (Fan et al., 2020; Isaacman-Vanwertz et al., 2016;

110 Nguyen et al., 2015). ~~As a result, there remain large uncertainties in identifying the anthropogenic~~

111 ~~influence on iSOA formation in ambient air.~~Furthermore, while the iSOA polyol tracers are formed in

112 the particle phase, they can actively partition between gas and particle phases due to their semi-volatile

113 characteristics (Fan et al., 2020; Isaacman-Vanwertz et al., 2016; Nguyen et al., 2015). As a result,

114 considering their particle-phase concentration only may bias our understanding of the atmospheric

115 abundance and chemistry of iSOA.

116   In recent years, great changes have taken place in air pollutant emissions, atmospheric composition,

117 and air quality in China due to the implementation of stringent clean air policies nationwide. For

118 example, $PM_{2.5}$ mass concentrations dropped significantly, with a notable reduction in inorganic water-

119 soluble ions such as sulfate, ammonium, and cation ~~ion~~s (Liu et al., 2023a; Zheng et al., 2018; Liu et

120 al., 2023b; Geng et al., 2024), and a relatively small decrease in organic aerosol in eastern China in the

121 past decade (Liu et al., 2023a; Yao et al., 2023). The reduction of inorganic ions including sulfate and

122 non-volatile cations (Na^+, K^+, Ca^{2+} and Mg^{2+}) resulted in a significant decrease in LWC and a slight

123 increase in aerosol acidity in this region (Zhou et al., 2022). However, concentrations of VOCs and

124 ozone exhibited different trends, with a slight decrease for the former while the latter showing an

125 upward trend before 2018 and a slight declining trend after 2018 (Wang et al., 2022; Liu et al., 2023a;

126 Yao et al., 2023; Gong et al., 2025). The changing atmospheric conditions can affect both gas-phase and

127 particle-phase chemistry, as well as the gas-particle partitioning behavior of organics. However, how

128 the formation of biogenic SOA, such as iSOA, respond to the changes in anthropogenic emissions and

129 air pollution conditions in polluted regions remains poorly understood.

130   The aim of this study is to ~~comprehend~~ understand the atmospheric abundance and formation

131   mechanisms of iSOA under the influence of continuous anthropogenic emission reductions in eastern

132   China. Ambient $PM_{2.5}$ samples were collected at an urban site in megacity Shanghai in winter and

133   summer of 2015, 2019, and 2021. The concentrations of isoprene-derived polyols and OSs from both

134   HO_2- and NO_x-dominated pathways in $PM_{2.5}$ samples were measured using gas chromatography-mass

135   spectrometry (GC-MS) and high-resolution liquid chromatography-mass spectrometry (LC-MS),

136   respectively, with the aid of a suite of authentic and surrogate standards. The quantification errors of

137   iSOA tracers were evaluated and their gas-particle partitioning behaviors were considered. The relative

138   distribution of measured iSOA tracers from different pathways as well as their inter-annual and seasonal

139   variations were analyzed and compared to the calculated reaction efficiency of different pathways as

140   well as the simulated values using the Community Multiscale Air Quality (CMAQ) model, which helps

141   to constrain the formation mechanisms of iSOA and the key factors driving the inter-annual variation

142   of iSOA tracers.

143   **2. Materials and methods**

144   **2.1 Sampling and Chemical Analysis**

145   Ambient $PM_{2.5}$ samples were collected on the rooftop of a 20-m tall teaching building at Xuhui

146   Campus of Shanghai Jiao Tong University (31.201° N, 121.429° E) located in the urban center of

147   Shanghai, China. The site is impacted by a mixed commercial and residential area. The sampling

148   campaigns were conducted in summer (July 14 to August 9 in 2015; 14 July to 9 August 2019; 7 July

149   to 5 August 2021) and winter (6 January to 26 January 2016; 27 December 2018 to 16 January 2019;

150   22 December 2021 to 18 January 2022) of 2015, 2019, and 2021. Sampling started at 8:00 am local

151   time and lasted for 23 hours. A total of 138 $PM_{2.5}$ samples were collected on prebaked (550 ℃, 6 h)

152   quartz filters (18×23 cm^2, Whatman) using a high-volume sampler (HiVol 3000, Ecotech) at a flow

153   rate of 67.8 m^3 h^{-1}. All sampled filters were wrapped with prebaked aluminum foil and stored at -20 ℃

154   until analysis.

155   iSOA polyol tracers, included 2-MG, cis-2-methyl-1,3,4-trihydroxy-1-butene, trans-2-methyl-

156   1,3,4-trihydroxy-1-butene, and 3-methyl-2,3,4-trihydroxy-1-butene (cis-2-MTB, trans-2-MTB, and 3-

157   MTB, collectively named as C_5-alkene triols), as well as 2-methylthreitol and 2-methylerythritol

158 (collectively named as 2-MTs), were analyzed by a GC-MS. The details regarding the sample

159 preparation and analysis protocol are presented in Section S1 in the supplement. An example of the total

160 ion chromatograms (TIC) of iSOA polyol tracers is shown in Figure S1d. For iSOA polyol tracers,

161 surrogate standards including erythritol, ~~KPA~~ketopinic acid, and glycerol were used for quantifications

162 in a number of studies (Kang et al., 2018; Ding et al., 2014; Zhang et al., 2019; Fan et al., 2020). In this

163 study, concentrations of 2-MG and 2-methylerythritol were quantified using their authentic standards

164 (Toronto Research Chemicals, 99.8%), and C_5-alkene triols and 2-methylthreitol were quantified by 2-

165 methylerythritol. The uncertainty for C_5-alkene triols was estimated previously and their concentration

166 was found to be underestimated by 65% when 2-methylerythritol was used as the surrogate

167 standard(Frauenheim et al., 2022). Furthermore, the uncertainty of 2-methylthreitol quantified by 2-

168 methylerythritol was assumed to be negligible as the differences in the TIC response for homologues

169 are determined by carbon number, functional groups, and number of active hydrogen atoms that would

170 silylate (Stone et al., 2012).

171 The particulate iSOA OSs were analyzed by a LC-MS employing a reversed-phase column (C_{18},

172 2.1 mm ×100 mm, 1.7 μm, Waters). The sample extraction procedure and analysis protocol were

173 described in detail in our previous work (Wang et al., 2021). A brief summary is given in Section S2

174 and examples of total and extracted ion chromatograms of iSOA OSs are provided in Figure S1a-c. The

175 lactic acid sulfate (LAS) was used as a surrogate standard to quantify the 2-MT-OS and 2-MG-OS.

176 ~~Previous studies illustrated that the ESI efficiency is dependent on structures of species (Kebarle, 2000).~~

177 ~~More relevantly, Bryant et al.~~(Bryant et al., 2021) ~~showed that camphorsulfonic acid (CAS), another~~

178 ~~commonly used surrogate standard for the quantification of 2-MT-OS and 2-MG-OS (Wang et al.,~~

179 ~~2023b; He et al., 2014; Hettiyadura et al., 2015), is ionized 2.4 times more efficiently than 2-MT-OS~~

180 ~~and 12.4 times more than 2-MG-OS. In this study, the relative ionization efficiency of CAS vs. LAS~~

181 ~~was measured to estimate the quantification uncertainties of iSOA OSs, based on the reported relative~~

182 ~~ionization efficiency of CAS vs. iSOA OSs~~ (Bryant et al., 2021)~~. Our results showed that the CAS~~

183 ~~ionized 4.62 times more efficiently than LAS. Accordingly, LAS would ionize 1.9 times less efficiently~~

184 ~~than 2-MT-OS and 2.68 times more than 2-MG-OS. This suggests that the concentration of 2-MT-OS~~

185 ~~might be 48% lower than quantified using LAS, while that of 2-MG-OS was 168% higher than~~

186 quantified by LAS. Use of surrogate standards would lead to uncertainties in measured concentrations

187 of 2-MT-OS and 2-MG-OS (Bryant et al., 2020; Bryant et al., 2021), but not alter the inter-annual trend

188 of iSOA OSs.

2.2 Additional measurements and models

190 The concentrations of organic carbon (OC) and element carbon (EC) in filter samples were

191 measured using a thermal–optical multiwavelength carbon analyzer (DRI, Model 2015). The

192 concentration of organic mass (OM) was estimated by multiplying the OC by 1.6 (Tao et al., 2014). An

193 ion chromatograph (Metrohm MIC) was employed to determine water-soluble inorganic compounds

194 (e.g., sulfate, nitrate, chloride, ammonium, potassium ion, and calcium ion). –Temperature, relative

195 humidity (RH), as well as the concentrations of trace gases and $PM_{2.5}$ were measured at a meteorological

196 station and an air quality monitoring station several km away from the sampling site. The details of the

197 two stations were described in our previous study (Wang et al., 2021) state-controlled air quality

198 monitoring station on the Xuhui Campus of Shanghai Normal University, which is surrounded by

199 residential areas and commercial districts and 4.5 km southwest of the $PM_{2.5}$ sampling site of this work.

200 and tThe mean values of these meteorological parameters and pollutant concentrations are listed in

201 Table S1.

202 LWC, pH, and bisulfate concentration in aqueous aerosols were predicted by the ISORROPIA-II

203 thermodynamic model (Wang et al., 2021). The molar concentrations of particulate water-soluble

204 inorganic ions (including sulfate, nitrate, chloride, ammonium, potassium ion, and calcium ion),

205 temperature, and RH were input into the model, which was run in the forward mode for metastable

206 aerosols. As the predicted aerosol pH could be underestimated when using particle-phase concentrations

207 of ion species as inputs only (Hennigan et al., 2015), we adopted the pH values of 2015 and 2019 at a

208 nearby site reported by Zhou et al. (2022), who used both particulate inorganic ion concentrations and

209 gaseous ammonia as inputs of ISORROPIA-II. Additionally, the 2021 pH was predicted by the

210 ISORROPIA-II using particle-phase-only concentrations of ions as input due to lack of gas-phase NH_3

211 data. Previous studies have found that lacking gas-phase inputs of ammonia could lead to under-

212 prediction of pH using thermodynamic equilibrium models, such as ISORROPIA and E-AIM (Guo et

213 al., 2015; Song et al., 2018; Hennigan et al., 2015). Guo et al. (2015) found that the pH values were

214 underestimated by 1 unit on average in southeast US when using only aerosol ammonium data as inputs

215 in ISORROPIA model. Similarly, Song et al. (2018) found that a 10-fold increase in gas-phase NH_3

216 concentrations roughly corresponds to a 1 unit increase in pH in the ammonia-rich atmosphere like

217 Beijing. In addition, we found that aerosol pH in 2015 and 2019 predicted using aerosol ammonium

218 only as input in our study was on average 1 unit lower than that predicted using gas-plus-particle-phase

219 ammonia as input in Zhou et al. (2022). Thus, we inferred that the lack of gas-phase concentrations of

220 ammonia might lead to underestimation of pH by ~1 unit in the present study and increased the output

221 pH estimated using aerosol ammonium only as input by one unit to represent aerosol acidity in

222 2021.~~Additionally, by comparing the predicted pH values of 2015 and 2019 in this study with the~~

223 ~~reported values in Zhou et al. (2022) during the same observation period, we found that the aerosol pH~~

224 ~~predicted using gas + aerosol inputs was on average one unit larger than that using aerosol inputs only.~~

225 ~~Therefore, output pH values of 2021 in this study were increased by one unit to represent the aerosol~~

226 ~~acidity.~~

227 In addition, considering that iSOA polyol tracers are semi-volatile and water-soluble, which can

228 partition into OM or dissolve into aerosol liquid water, their gas-phase and particle-phase fractions were

229 estimated by accounting for the gas-organic phase partitioning using an organic absorptive equilibrium

230 partitioning model and the gas-aqueous phase partitioning using the Henry's Law. The details of the

231 estimation method are described in Section S3.

232 **2.3 Quality control and quality assurance**

233 Procedural blanks (run every 6 samples) and field blanks (two for each season) were extracted and

234 analyzed in the same manner as the $PM_{2.5}$ filter samples. Target compounds were found below the

235 detection limit in the blanks. The recovery of iSOA polyol tracers as represented by that of the internal

236 standard (ketopinic acid) during GC-MS analysis was determined to be 85±17% and the recovery of

237 iSOA OSs during LC-MS analysis was 72.5%, as determined using LAS spiked onto the filter in our

238 previous study (Wang et al., 2021).

239 As the $PM_{2.5}$ sample extracts contain thousands of multifunctional compounds, there might exist

240 a significant matrix effect in the analysis of iSOA tracers. The matrix effect of polyol tracers was

241 evaluated by comparing the signal responses of authentic standards of 2-methylerythritol and 2-MG in

242   PM$_{2.5}$ extracts to those in pure solvent. Six filter samples representing low and high PM$_{2.5}$ concentrations

243   in summer and winter were used to test the matrix effect. 16 μL or 160 μL of 2-methylerythritol and 2-

244   MG standard mixtures (10 ppm) was added to the filter extracts to represent the low and high

245   concentrations of 2-methylerythritol and 2-MG in the samples. The filters were subsequently analyzed

246   as described in Section 2.~~2~~1. The matrix factors of the standards were calculated as the ratio of their

247   signal response in sample extracts (the signal response of these species in non-spiked extracts was

248   subtracted) to their signal response in the pure solvent. As shown in Table S2, 2-MG had a matrix factor

249   of 0.77 ± 0.12, while that of 2-methylerythritol was 1.24 ± 0.08, indicating that the concentrations of 2-

250   MG were likely underestimated by 23% whereas 2-methylerythritol was overestimated by 24% due to

251   the matrix effect.

252   ~~For OS tracers,~~ Bryant et al. (2021) ~~have assessed the matrix effect of 2-MT-OS and 2-MG-OS~~

253   ~~using authentic standards and found that the matrix factors were 0.29 ± 0.23 and 0.84 ± 0.18~~(Bryant et

254   al., 2021)~~, respectively. If similar matrix effects for 2-MT-OS and 2-MG-OS reported by~~ Bryant et al.

255   (2021)~~ occurred in our measurements, the concentrations of these two OS species would be~~

256   ~~underestimated by 71% and 16%, respectively.~~ Previous studies have demonstrated that the

257   concentrations of 2-MT-OS and 2-MG-OS were significantly underestimated due to matrix effect by

258   using reversed phase liquid chromatography-mass spectrometry (RPLC-MS) (Hettiyadura et al., 2015;

259   Bryant et al., 2020; Bryant et al., 2021). In the present work, because of lack of authentic standards of

260   isoprene-derived OSs, we are not able to quantify the absolute value of underestimation in the

261   concentration of 2-MT-OS and 2-MG-OS due to the matrix effect. However, using ambient PM$_{2.5}$

262   samples with different concentrations, we can quantify the relative extent of underestimation in OS

263   concentrations due to matrix effect in different samples, which allows for an evaluation of uncertainties

264   in the abundance, trend, and relative ratios of different iSOA tracers in this study. In the matrix effect

265   experiments, the extracts of ambient PM$_{2.5}$ samples with different concentrations were mixed and the

266   measured signals of 2-MT-OS and 2-MG-OS in mixed extracts were compared to the sum of OS signals

267   detected separately in individual extracts. The concentrations of PM$_{2.5}$, sulfate, as well as 2-MT-OS and

268   2-MG-OS in ambient samples used for this evaluation are listed in Table S3. The relative matrix effect

269   factor (F$_{matrix}$), defined as the ratio of the measured OS signals in mixed extracts to the sum of OS signals

270 measured in each extract before mixing, are used to evaluate the matrix effects of OSs. A F_{matrix} value

271 of less than 1 indicates the presence of matrix effect.Bryant et al. (2021) Bryant et al. (2020)

272   As shown in Figure S2, the F_{matrix} values were significantly smaller than 1 in both summer and

273 winter, indicating that the signal responses of 2-MT-OS and 2-MG-OS in mixed extracts were largely

274 suppressed due to the matrix effect. Notably, F_{matrix} exhibits a significant negative dependence on the

275 reduced mass (μ, $\mu g\ m^{-3}$), a proxy used to represent effective mass loadings of the mixed $PM_{2.5}$ extracts,

276 defined as:

$$\mu = \sqrt{m_1 * m_2/(m_1 + m_2)} \tag{1}$$

278 where m_1 and m_2 are the $PM_{2.5}$ mass loading of individual samples. This observation suggests that the

279 concentrations of iSOA OSs in $PM_{2.5}$ samples collected in 2015 were underestimated more than those

280 in 2021, given that ambient $PM_{2.5}$ concentrations declined by 39.8% and 47.0% from 2015 to 2021 in

281 summer and winter, respectively.

282   As $PM_{2.5}$ concentrations in ambient samples used for the matrix effect evaluation generally

283 represent lower or upper ends of $PM_{2.5}$ concentrations during the observation period (see Table S3), the

284 relative differences in measured F_{matrix} values at varying reduced mass (Figure S32) may roughly reflect

285 the differences in the extent of underestimation in OS concentrations for samples collected across 2015-

286 2021. During summer, the F_{matrix} value decreased from 0.71 to 0.63 for 2-MT-OS and from 0.85 to 0.58

287 for 2-MG-OS with increasing reduced mass, indicating that the concentrations of these two iSOA OSs

288 were a factor of 1.2 and 1.5 more underestimated in 2015 than in 2021 due to matrix effect. Similarly,

289 during winter the F_{matrix} values of iSOA OSs decreased from 0.9 to 0.6 with rising reduced mass,

290 implying a factor of 1.5 greater underestimation in OS concentrations in 2015 than in 2021.

2.4 Estimation of the reaction efficiency of isoprene-derived epoxides in aqueous aerosols

292   The IEPOX/HMML/MAE can undergo acid-catalyzed nucleophilic addition with water and sulfate

293 to form polyol tracers (2-MTs and 2-MG) and OSs (2-MT-OS and 2-MG-OS) in aqueous aerosols,

294 respectively. The aqueous-phase pseudo-first-order rate constants (k_{aq}, s^{-1}) for epoxides could be

295 estimated by eq 1 (Eddingsaas et al., 2010),

$$k_{aq} = \sum_{i=1}^{N} \sum_{j=1}^{M} k_{ij} [nuc_i]_{aq} [acid_j]_{aq} \tag{12}$$

297 Where k_{ij} is the third-order reaction rate constant of isoprene-derived epoxides with nucleophile i

298   (water or sulfate) and acid j (hydrogen ion or bisulfate) in the aqueous phase and the reported values of

299   k_{ij} in previous studies are shown in Table 1. When epoxides react with water and sulfate, the aqueous-

300   phase reaction rate constants ($k_{aq,\ H_2O}$ and $k_{aq,\ SO_4^{2-}}$) can be estimated by eqs 2 and 3, respectively.

301
$$k_{aq,\ H_2O}=k_{H_2O,H^+}[H_2O]_{aq}\left[H^+\right]_{aq}+k_{H_2O,HSO_4^-}[H_2O]_{aq}[HSO_4^-]_{aq} \tag{23}$$

302
$$k_{aq,\ SO_4^{2-}}=k_{SO_4^{2-},H^+}\left[SO_4^{2-}\right]_{aq}\left[H^+\right]_{aq}+k_{SO_4^{2-},HSO_4^-}\left[SO_4^{2-}\right]_{aq}[HSO_4^-]_{aq} \tag{43}$$

303   Where $\left[H^+\right]_{aq}$, $[HSO_4^-]_{aq}$, and $[H_2O]_{aq}$ are molar concentrations of hydrogen ion, bisulfate, and

304   ALWC in aqueous aerosols, which were estimated by ISORROPIA-II model, and $\left[SO_4^{2-}\right]_{aq}$ is the molar

305   concentration of sulfate.

306   The reactive uptake coefficient (γ) of epoxides on aqueous aerosols is parameterized by a resistor

307   model (Xu et al., 2016; Pye et al., 2013).

308
$$\frac{1}{\gamma}=\frac{1}{\alpha}+\frac{\omega}{4H_{epoxide}RT\sqrt{D_ak_{aq}}}\frac{1}{f(q)} \tag{54}$$

309
$$f(q)=\coth(q)-\frac{1}{q} \tag{65}$$

310
$$q=r_p\sqrt{k_{aq}/D_a} \tag{76}$$

311   Where r_p is the particle radius. Previous work has found that the surface area (S_a, m^2 m^{-3}) and volume

312   concentrations (V_a, m^3 m^{-3}) of dry PM$_{2.5}$ could be described as a function of PM$_{2.5}$ mass concentration

313   ($C_{PM_{2.5}}$, μg m^{-3}) in Shanghai (S_a=7.54×10^{-6}•$C_{PM_{2.5}}$+1.01×10^{-4}, V_a=5.59×10^{-13}•$C_{PM_{2.5}}$+1.02×10^{-12})

314   (Zang et al., 2022). In this study, the mean particle radius of dry PM$_{2.5}$ was calculated as $3V_a/S_a$, which

315   was then corrected for the aerosol hygroscopic growth to get the wet particle radius based on the κ-

316   Köhler hygroscopicity function (see details in Section S4). α is the mass accommodation coefficient

317   taking a value of 0.02 for both IEPOX and HMML&/MAE (Mcneill et al., 2012), ω is the mean

318   molecular velocity of epoxides, H$_{epoxide}$ is the Henry's law constant in the aqueous phase, with a value

319   of 2.7 × 10^6 M atm^{-1} for IEPOX (Pye et al., 2013) and a constrained value of 7.5 × 10^6 M atm^{-1} for

320   HMML&/MAE by CMAQ in Case 1, and k$_{aq}$ is the first-order reaction rate constant in the aqueous

321   phase (s^{-1}), estimated using eq 1.

322 To describe the overall loss rate of gas-phase epoxides due to the reactive uptake by aqueous

323 aerosols, the pseudo-first-order heterogeneous reaction rate constant was calculated by eq 7, when

324 neglecting the gas-phase diffusion limitation:

325 $$k_{het} = \gamma \omega S_a / 4 \tag{87}$$

326 **2.5 Model Simulations**

327 The CMAQ model (v5.2) was adopted to simulate the gas-phase concentration of isoprene and

328 particulate concentrations of 2-MTs, 2-MG, and their OS derivatives formed involving the reactive

329 uptake of IEPOX and HMML&/MAE on aqueous aerosols (Pye et al., 2017) in both summer and

330 winter of 2015 and 2019 in Shanghai. The simulations performed with the standard CMAQ v5.2 are

331 referred to as the Base Case. While the advanced model simulations performed according to a recent

332 study by Zhang et al. (2023) are named as Case 1. In this advanced case, the iSOA polyol tracers were

333 treated as semi-volatile species that partition between gas, aqueous, and organic phases, while the OS

334 tracers were treated as non-volatile species. The removal of iSOA polyol tracers by OH radicals in the

335 gas and particle phases was also considered. The key parameters for simulating reactive uptake of

336 IEPOX/HMML&/MAE and the removal of 2-MTs and 2-MG in the gas phase and aqueous aerosol in

337 the model are listed in Table S3 S4 and S4S5.

338 In this work, three nested domains covering mainland China, eastern China, and the Yangtze

339 River Delta were configured with horizontal resolutions of 36 km × 36 km (d01), 12 km × 12 km (d02),

340 and 4 km × 4 km (d03), as shown in Figure S2S3. The outermost domain (d01) was driven by

341 predefined initial and boundary conditions from CMAQ, with its outputs supplying these conditions

342 for d02, which in turn provided them for d03. All domains employed a vertical structure consisting of

343 18 layers, extending from the surface to an altitude of 21 km.

344 Anthropogenic emissions were sourced from the Multi-resolution Emission Inventory for China

345 (MEIC) version 1.4 for China (Geng et al., 2024) and the Regional Emission inventory in ASia (REAS)

346 version 3.2.1 for other Asian countries and regions (Kurokawa and Ohara, 2020). Open biomass

347 burning emissions were based on the Fire INventory from NCAR (FINN) version 2.5 (Wiedinmyer et

348 al., 2023). Biogenic emissions were estimated using the Model of Emissions of Gases and Aerosols

349 from Nature (MEGAN) version 2.1, incorporating the high-quality Leaf Area Index (HiQ-LAI) dataset

350 developed by Yan et al. (2024), which enhances the spatiotemporal consistency of MODIS LAI

351 products. Meteorology data was generated by the Weather Research and Forecasting (WRF) model

352 version 4.2.1 with initial and boundary conditions from the fifth generation ECMWF atmospheric

353 reanalysis data (ERA5).

354   The simulation was conducted for four periods: 12 July–9 August 2015, 25 December 2015–16

355 January 2016, 4–26 January 2019, and 12 July–5 August 2019. The first two days of each period were

356 treated as spin-up periods and excluded from the analysis.

357 **3. Results and Discussion**

358 **3.1 Temporal evolution of major air pollutants during the observation period**

359   Time series of $PM_{2.5}$ and its major components, as well as the major trace gases (NO_2 and O_3) and

360 meteorological parameters during the observation period are shown in Figure 1 and ~~the seasonal and~~

361 ~~inter-annual variations of various pollutants are further demonstrated in Figure 2~~their seasonally

362 averaged values are presented in Table S1. The concentration of NO_2 exhibited an obvious downward

363 trend, in particular in summer from 2015 to 2021, consistent with a strong reduction in anthropogenic

364 emissions during this period. By contrast, ~~the concentration of O_3 significantly decreased from 52.0 ±~~

365 ~~38.9 ppb in 2015 to 41.2 ± 22.8 ppb in 2019 (p < 0.05) and then remained at a comparable level (43.4~~

366 ~~± 20.8 ppb) in 2021~~O_3 showed a more complex inter-annual trend, with the average concentration

367 dropped from 52.0 ± 38.9 ppb in 2015 to 41.2 ± 22.8 ppb in 2019 (p < 0.05), but then increased to 43.4

368 ± 20.8 ppb in 2021, suggesting a complex response of secondary O_3 formation to primary emission

369 reductions. During the observation period, ~~the average $PM_{2.5}$ concentration decreased by 41.7% from~~

370 ~~2015 to 2021, with concentrations of major components, including sulfate, ammonium, and OM,~~

371 ~~decreasing by 51.8%, 40.6%, and 39.1%, respectively (Figure 2)~~ the concentrations of $PM_{2.5}$, most of

372 the inorganic ions (sulfate, chloride, and ammonium), and OM exhibited a dramatic descending trend

373 in both seasons (see Table S1). In contrast, the concentration of ~~aerosol~~ nitrate showed a slight upward

374 trend during this period, in line with the measurement in urban Shanghai by Zhou et al. (2022). Overall,

375 OM was the most abundant component in $PM_{2.5}$, accounting for 10.2-72.7% (average 22.6%) of total

376 $PM_{2.5}$ mass, followed by sulfate (6.8-45.2%, average 17.7%), nitrate (0.5-32.6%, average 17.0%), and

377 ammonium (1.1-18.2%, average 8.8%)~~Overall, OM was the most abundant component in $PM_{2.5}$,~~

378   ~~accounting for 10.2-72.7% of total PM$_{2.5}$ mass, followed by sulfate (6.8-45.2%), nitrate (0.5-32.6%),~~

379   ~~and ammonium (1.1-18.2%).~~ Ascribed to the strong decrease of inorganic ion concentrations (in

380   particular sulfate), aerosol LWC decreased from 9.14 ± 4.51 μg m^{-3} in 2015 to 4.40 ± 2.76 μg m^{-3} in

381   2021 ~~aerosol LWC decreased dramatically from 2015 to 2021~~($p < 0.05$). Aerosol pH decreased from

382   3.2 ± 0.4 in 2015 to 2.5 ± 0.9 in 2021 ($p < 0.05$), which was mainly driven by the decrease of non-

383   volatile cations during these years, though the decreased concentrations of sulfate had an opposite effect

384   on aerosol acidity (Zhou et al., 2022).

385

386
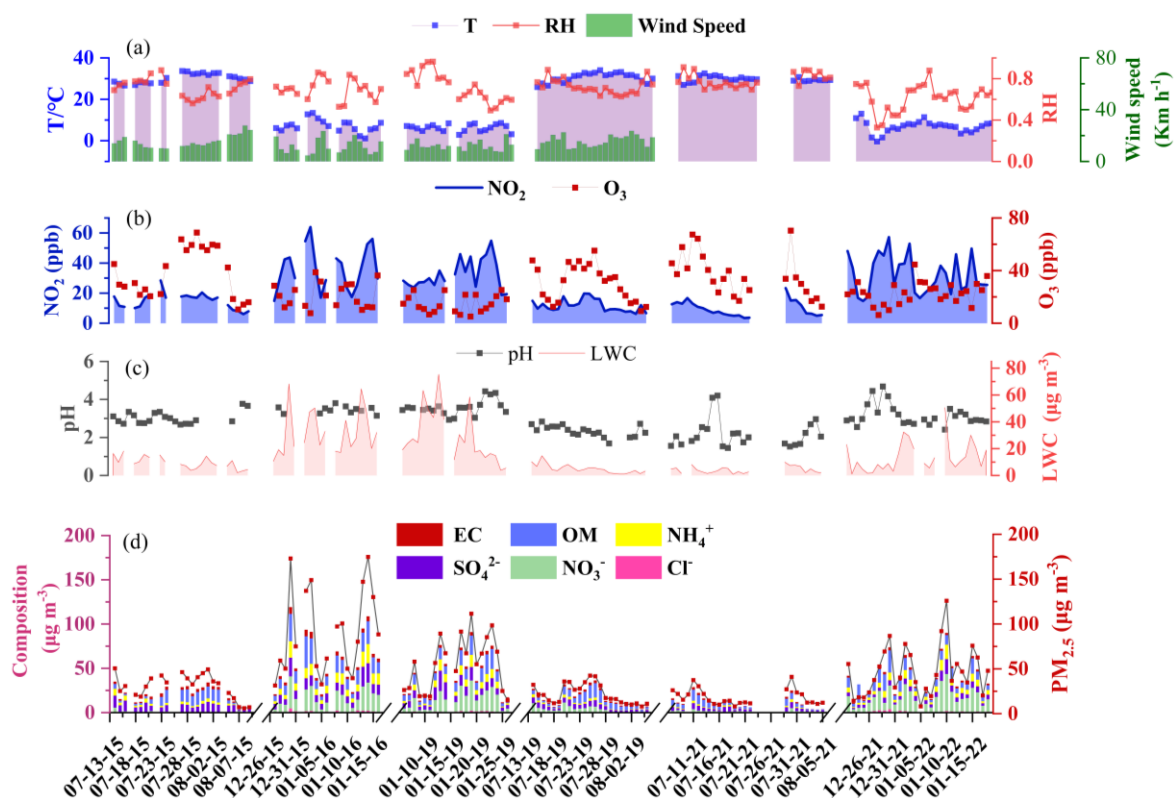
Figure 1. Temporal variations of (a) meteorological parameters (ambient temperature, relative humidity, and wind speed), (b) concentrations of NO$_2$ and O$_3$, (c) aerosol pH and liquid water content (LWC), and (d) concentrations of PM$_{2.5}$ and its major components (OM, EC, sulfate, nitrate, chloride, and

390 ammonium) in urban Shanghai during the observation period. The wind speed data were not collected

391 during the observations in 2021.

3.2 Seasonal and annual variations of iSOA tracers

393   The measured concentrations of particulate iSOA tracers during the observation period are

394 summarized in Figure 2 and their specific concentration values are also provided in Table S1. Among

395 the measured iSOA tracers, C_5-alkene triols were the most abundant species with average concentrations

396 of 27.6 ng m^{-3} in 2015, 20.9 ng m^{-3} in 2019, and 11.1 ng m^{-3} in 2021, accounting for 28.8 %, 22.4, and

397 18.7 % of the total iSOA mass, followed by 2-MT-OS, 2-MTs, 2-MG-OS, and 2-MG. However, the

398 concentrations of C_5-alkene triols might be overestimated since previous studies have reported that

399 concentrations of C_5-alkene triols could be artifacts of thermal degradation products of 3-

400 methyltetrahydrofuran-2,4-diols and 2-MT-OS during GC/MS analysis (Cui et al., 2018; Frauenheim et

401 al., 2022). Frauenheim et al. (2022) found that less than 15% of 3-methyltetrahydrofuran-2,4-diols could

402 transfer to two isomers of C_5-alkene triols (cis-/trans-3-methyl-but-3-ene-1,2,4-triols). In the present

403 study, using 2-methylerythritol as a surrogate standard, the concentrations of 3-methyltetrahydrofuran-

404 2,4-diols were determined to be less than 5% of C_5-alkene triols in summer but had comparable

405 concentrations to C_5-alkene triols in winter. This result indicates that 3-methyltetrahydrofuran-2,4-diols

406 was a minor contributor to C_5-alkene triols in summer but an important source for C_5-alkene triols in

407 winter. In contrast, the contribution from the thermal degradation of 2-MT-OS might be more significant,

408 though the specific contribution remains to be quantified; Cui et al. (2018) found that thermal

409 degradation of 2-MT-OS could generate all three isomers of C_5-alkene triols, while (Yee et al., 2020)

410 found that the thermal decomposition of 2-MT-OS could only produce one isomer, 3-methyl-2,3,4-

411 trihydroxy-1-butene. Given these uncertainties, it is difficult to quantitatively evaluate the artifact

412 formation of C_5-alkene triols during GC/MS analysis. Therefore, the abundance and inter-annual trend

413 of C_5-alkene triols were not discussed in detail in the present work.

414   As shown in Figure 2, Tthe particle-phase concentrations of total and specific IEPOX-SOA tracers

415 (except 2-MTs) decreased yearly in both summer and winter between 2015-2021 (Figs. 2a-d), while the

416 particulate concentrations of total and specific HMML&/MAE-SOA species did not show a significant

417 inter-annual trend in summer during this period (Figs. 2e-g). However, the inter-annual trend of iSOA

418   OSs could be altered due to the matrix effect. The measured concentration of 2-MT-OS exhibited a

419   decreasing inter-annual trend, while 2-MG-OS showed insignificant variation between 2015-2021.

420   Accounting for the significantly larger matrix effects in 2015 samples compared to 2021 samples (see

421   Section 2.3), the true concentrations of 2-MT-OS would decrease more sharply and 2-MG-OS might

422   also exhibit a declining trend. Recently, Frauenheim et al. (2024) demonstrated that gas-phase OH

423   oxidation of 3-methylenebutane-1,2,4-triol (3-MBT) and 3-methyltetrahydrofuran-2,4-diols, formed

424   from acid-catalyzed isomerization of IEPOX in aerosols, can yield 2-MT-OS and 2-MG-OS. However,

425   in the present study, the gas-phase concentrations of 3-MBT and 3-methyltetrahydrofuran-2,4-diols

426   were not measured, precluding a quantitative assessment of the contribution of their oxidation products

427   to 2-MT-OS and 2-MG-OS. Given that IEPOX-SOA concentrations observed here exhibited a

428   significant decreasing trend over the observation period, the concentrations of IEPOX isomerization

429   products, such as 3-MBT and 3-methyltetrahydrofuran-2,4-diols, likely also decreased annually.

430   Therefore, gas-phase OH oxidation of these species might represent a plausible contributor to the inter-

431   annual decline in 2-MT-OS and 2-MG-OS.

432
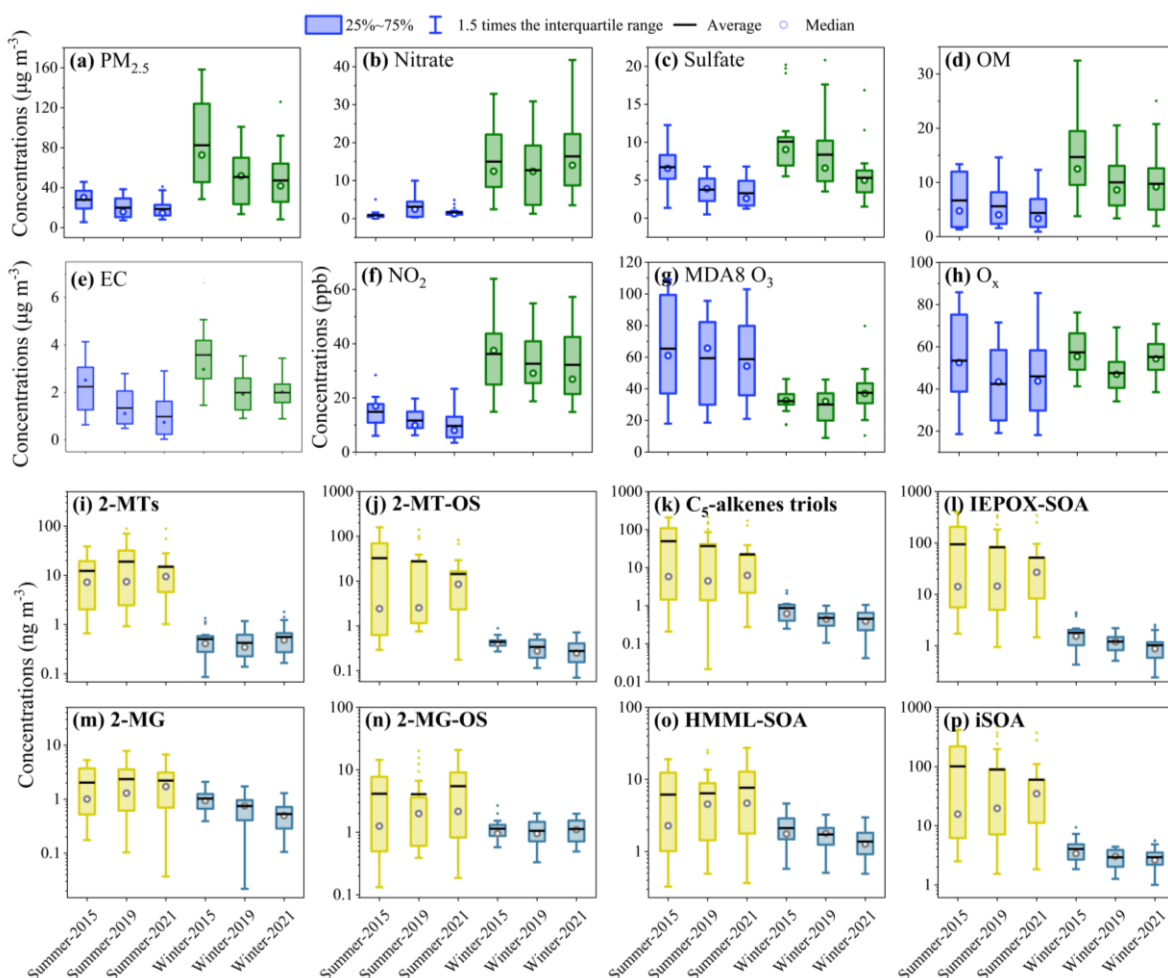
433 Figure 2. Seasonal and inter-annual variations concentration of PM₂.₅ and its major components (a-e),

434 gas-phase anthropogenic pollutants (f-h), as well as particulate iSOA tracers, including (i)2-MTs, (j) 2-

435 MT-OS, (k) C₅-alkene triols, (l) IEPOX-SOA (the sum of 2-MTs, 2-MT-OS, and C₅-alkene triols), (m)

436 2-MG, (n) 2-MG-OS, (o) HMML&MAE-SOA (2-MG plus 2-MG-OS), and (p) iSOA (the sum of all

437 tracers)~~in particulate concentrations of (a) 2-MTs, (b) 2-MT-OS, (c) C₅-alkene triols, (d) IEPOX-SOA~~

438 ~~(the sum of 2-MTs, 2-MT-OS, and C₅-alkene triols), (e) 2-MG, (f) 2-MG-OS, (g) HMML/MAE-SOA~~

439 ~~(2-MG plus 2-MG-OS), and (h) iSOA (the sum of all tracers)~~.

440

441 The particulate concentrations of IEPOX-SOA (52.6 ± 97.6, 46.7 ± 103.8, and 25.8 ± 62.9~~94.1, 82.3,~~

442 ~~and 51.7~~ ng m⁻³ in 2015, 2019 and 2021, respectively) dominated over HMML&~~/~~MAE-SOA (6.2 ± 6.4,

443 6.4 ± 7.0, and 7.7 ± 7.7 ng m⁻³) in summer, while ~~the concentrations of IEPOX-SOA~~ they were ~~slightly~~

444 ~~lower than~~comparable to HMML&~~/~~MAE-SOA in winter. Although C₅-alkene triols might be largely

445 artifacts of GC/MS analysis (Cui et al., 2018; Frauenheim et al., 2022), the concentrations of IEPOX-

446   SOA excluding C_5-alkene triols were still dominant over HMML&MAE-SOA in summer. In addition,

447   previous studies have demonstrated that the concentrations of 2-MT-OS were underestimated more than

448   2-MG-OS by a factor of 5.7-9.1 in Beijing (Bryant et al., 2020) and 2.9 in Guangzhou (Bryant et al.,

449   2021). If 2-MT-OS was also more significantly underestimated than 2-MG-OS in the present study, the

450   predominance of IEPOX-SOA over HMML&MAE-SOA would be more pronounced. The dominance

451   of IEPOX-SOA over HMML&MAE-SOA in summer is in agreement with RPLC-MS measurements in

452   Beijing, Hefei and Kunming in China (Zhang et al., 2022) and Birmingham, US (Rattanavaraha et al.,

453   2016), as well as hydrophilic interaction liquid chromatography-mass spectrometry (HILIC-MS)

454   measurements conducted in urban Guangzhou, China (Liu et al., 2025). ~~The dominance of IEPOX-SOA~~

455   ~~over HMML/MAE-SOA in summer is in agreement with field studies conducted in Beijing, Hefei and~~

456   ~~Kunming in China (Zhang et al., 2022) and Southeastern US (Budisulistiorini et al., 2015;~~

457   ~~Rattanavaraha et al., 2016; Lin et al., 2013a).~~

458   The annual average particulate concentration of the total iSOA polyol tracers (including 2-MTs, 2-

459   MG, and C_5-alkene triols) were 36.1 ± 63.3, 33.4 ± 70.5, and 18.7 ± 47.1~~36.1, 33.4, and 18.7~~ ng m^{-3} in

460   2015, 2019 and 2021, higher than those of OS tracers (including 2-MT-OS and 2-MG-OS) by a factor

461   of 2.5, 2.1, and 1.4, respectively. ~~The dominance of iSOA polyol tracers over OS tracers is in agreement~~

462   ~~with observations in other urban regions~~ (Zhang et al., 2022; He et al., 2018). However, given the

463   significant underestimation of iSOA OSs due to matrix effect and overestimation of C_5-alkene triols

464   due to their potential artifact formation, the true concentration of iSOA OSs would predominate over

465   that of polyol tracers. The iSOA OSs prevailing over polyol tracers is consistent with urban observations

466   using HILIC-MS, such as in Manaus, Brazil (Cui et al., 2018) and Guangzhou, China (Liu et al., 2025)

467   (see Table S6). Using RPLC-MS, Bryant et al. (2020) also observed higher concentrations of iSOA OSs

468   than polyol tracers in Beijing, China. Considering the potential underestimation of iSOA OSs due to

469   matrix effect, the concentration of iSOA OSs would be even higher than that of polyol tracers in their

470   study.

471   ~~The particle phase concentrations of total and specific IEPOX-SOA tracers (except 2-MTs)~~

472   ~~decreased yearly in both summer and winter between 2015-2021 (Figs. 2a-d), while the particulate~~

473   ~~concentrations of total and specific HMML/MAE-SOA species did not show a significant inter-annual~~

trend in summer during this period (Figs. 2e–g). 2-MTs exhibited a different inter-annual trend compared to other IEPOX-SOA tracers (Figure 2i). A possible explanation for this discrepancy is that 2-MTs may have origins other than reactive uptake of IEPOX on aqueous aerosol. Previous studies have found that 2-methylerythritol, one isomer of 2-MTs, could be generated by biosynthetic pathways (Duvold et al., 1997; Sagner et al., 1998; Rohmer, 1999; Lange et al., 2000; Yang et al., 2013). And the contributions of non-IEPOX pathway to 2-MTs concentrations were pH-dependent, accounting for 20-40% in areas with aerosol pH < 2 and more than 70% under less acidic conditions (pH ~ 2–5) (Zhang et al., 2023). The contribution of biological emissions to 2-MTs might be important in Shanghai given its less acidic aerosol conditions (pH > 2). As a whole, the particulate concentrations of iSOA decreased significantly in both seasons from 2015 to 2021. In addition, all iSOA compound classes had substantially higher concentrations in summer than in winter. Such a strong seasonality in abundance is mainly driven by the higher temperature and stronger solar radiation, and thereby more intensive isoprene emissions and photochemistry in summer than in winter. Notably, HMML&/MAE-SOA species exhibited a relatively smaller seasonal variation than IEPOX-SOA. This is partially owing to the fast thermolysis of methacryloyl peroxynitrate (MPAN) in summer, reducing the formation of HMML&/MAE and thereby SOA (Worton et al., 2013).

To further investigate factors that affect the abundance of iSOA, the particulate concentrations of 2-MTs, 2-MT-OS, 2-MG, and 2-MG-OS, as well as the gas-phase concentration of isoprene were simulated with the CMAQ model and compared to measurements in summertime and wintertime of 2015 and 2019 (see Figure 3). Predicted concentrations of isoprene were generally consistent with observations with a median correlation (r^2=0.45), except in the summer of 2015, during which isoprene concentrations were significantly overestimated (Figure 3a). For iSOA tracers, the Case 1 showed a better prediction than the Base Case. Overall, the simulated IEPOX-SOA tracers were biased low in summer, but biased high in winter (Figure 3b and 3c)., though the isoprene precursor was overestimated more in summer than in winter. This result indicates that the chemical process or transport, rather than the precursor, plays a critical role in controlling the variations in iSOA concentrations. HoweverIn contrast, the 2-MG and 2-MG-OS were biased low in both seasons (Figure 3d and 3e)–. The underestimation of 2-MG is consistent with previous simulations at 14 sites across China in the summer

502 of 2012 (Qin et al., 2018). ~~which is in consistent with previous simulations at 14 sites across China in~~

503 ~~summer (Qin et al., 2018).~~ Accounting for the underestimation of OSs due to the matrix effect, simulated

504 concentrations of 2-MT-OS would be more biased low in summer but might be close to observations in

505 winter. Similarly, the under-prediction of 2-MG-OS would be more significant in both seasons. The

506 larger uncertainty of simulated HMML~~/~~&MAE-SOA tracers compared to that of IEPOX-SOA might be

507 attributed to the lack of well constrained kinetic parameters for reactive uptake of HMML~~/~~ and MAE.

508 In addition, simulated concentrations of iSOA tracer species had decreasing inter-annual trend in both

509 Base Case and Case 1 (Figure ~~S3~~S4), which was in agreement with observations of total iSOA, 2-MT-

510 OS, and 2-MG-OS (with matrix effect considered), but not for 2-MG and 2-MTs. ~~total iSOA and IEPOX~~

511 ~~SOA, but not for HMML/MAE-SOA species.~~ ~~This~~ These result~~s~~ suggest~~s~~ that the major factors driving

512 the overall formation and evolution of iSOA and in particular ~~IEPOX-SOA~~ iSOA OSs were captured

513 by the model, while some factors governing the abundance of 2-MG and 2-MTs ~~HMML/MAE-SOA~~

514 might not be well represented in the model.

515
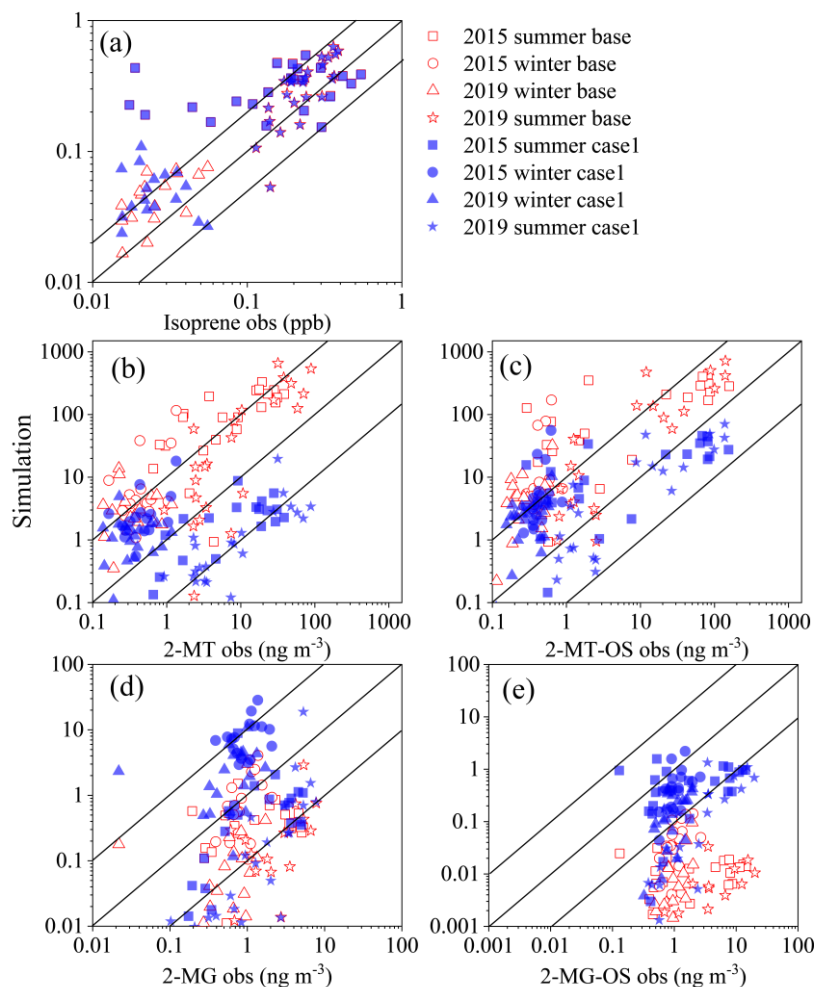
Figure 3. Comparisons of simulations against observations for (a) isoprene, (b) 2-MTs, (c) 2-MT-OS, (d) 2-MG, (e) 2-MG-OS in summer and winter of 2015 and 2019. Red dot represents simulations with standard CMAQ v5.2 (Base Case), and blue represents simulations using the optimized model (Case 1). The 1:1, 10:1, and 1:10 lines are shown with solid lines.

The gas-phase and particle-phase fractions of 2-MG and 2-MTs were estimated using a chemical equilibrium partitioning model as described in Section S3 and the results are shown in Figure S4S5. The particle-phase fraction (F_p) of 2-MG was highly variable, with a significant lower value in summer (9.0 -19.0%) than in winter (31.6 - 44.0%), indicating substantial amounts of 2-MG was present in the gas phase in summer. Additionally, the F_p value of iSOA polyols, in particular for 2-MG, decreased yearly. As a result, the gas-plus-particle-phase concentrations of 2-MG showed an upward trend in summer from 2015-2021 ($p < 0.05$, Figure S4S5). In contrast, 2-MTs were mainly distributed in the particle phase with F_p values larger than 70% in both seasons, consistent with previous measurements

528 (Isaacman-Vanwertz et al., 2016). The inter-annual trend of 2-MTs was not significantly affected by

529 their gas-phase fraction because of the relatively low volatility. ~~Overall, the total HMML/MAE-SOA~~

530 ~~exhibited a distinctly different inter-annual trend compared to IEPOX-SOA in summer over 2015-2021.~~

531 ~~It should be noted that although the measured concentrations of iSOA tracers could be affected by~~

532 ~~quantification uncertainties including matrix effect and the use of surrogate standards, their inter-annual~~

533 ~~trends were not affected by these uncertainties.~~ Overall, compared to other iSOA tracers in summer, 2-

534 MG and 2-MTs exhibited a distinctly different inter-annual trend over 2015-2021. It should be noted

535 that the use of surrogate standards would not alter the trend of iSOA tracers. The key factors driving

536 such trends will be discussed in detail ~~in Sections 3.2 and 3.3~~below.

537 ~~As shown in Table S1, the concentration ratios of IEPOX-SOA to HMML/MAE-SOA in the~~

538 ~~particle phase decreased in both summer (11.1 ± 6.7, 7.8 ± 6.3, and 5.6 ± 3.0 in 2015, 2019, and 2021,~~

539 ~~respectively) and winter (0.8 ± 0.3, 0.8 ± 0.2, and 0.7 ± 0.4). This result indicates an increasing~~

540 ~~contribution of NOₓ-influenced pathways to iSOA formation despite the strong anthropogenic emission~~

541 ~~reductions from 2015 to 2021 in Shanghai. Accounting for the gas-particle partitioning of 2-MTs and~~

542 ~~2-MG as well as the quantification uncertainties for iSOA tracers do not significantly change such a~~

543 ~~decreasing trend. However, it significantly decreases the ratio values of IEPOX-SOA to HMML/MAE-~~

544 ~~SOA to 2.63 ± 1.93, 1.55 ± 2.15, and 0.90 ± 0.81 in summer and 0.39 ± 0.15, 0.33 ± 0.11, and 0.29 ±~~

545 ~~0.17 in winter of 2015, 2019, and 2021, respectively, suggesting that the corrected gas-plus-particle-~~

546 ~~phase concentration of HMML/MAE-SOA tracers was comparable to that of IEPOX-SOA tracers. This~~

547 ~~result emphasizes the importance of considering the gas-particle partitioning of polyols for a deeper~~

548 ~~understanding of the abundance and formation characteristics of iSOA.~~

549 **3.3 Key influencing factors of iSOA formation**

550 The production of iSOA can be influenced by a variety of factors such as the emission and

551 concentration of isoprene, atmospheric oxidizing capacity as represented by the concentrations of O_3 or

552 odd oxygen ($O_x = O_3 + NO_2$), nitrogen oxides, as well as aerosol composition and properties including

553 sulfate content, acidity, and LWC. Here, we identify the major influencing factors of IEPOX-SOA and

554 HMML&/MAE-SOA formation through the correlation analysis between different iSOA tracers and

555 influencing factors (Figure 4).

556   The correlations of all iSOA species with isoprene were relatively weak, with most of the

557   correlation coefficients (r^2) below 0.37. Therefore, the decline in iSOA concentrations from 2015 to

558   2021 could not be attributed to the slight variation in isoprene concentration. The HMML&/MAE-SOA

559   species exhibited strong correlations with ozone ($r^2 = 0.48\text{-}0.81$) and O_x ($r^2 = 0.57\text{-}0.82$) in summer, in

560   particular in 2015 and 2021 while exhibiting relatively weaker correlations with NO_2 ($r^2 = 0.20\text{-}0.55$).

561   Such correlations between 2-MG and ozone were also observed in previous measurements in urban

562   areas in southeastern US (Rattanavaraha et al., 2016), which proposed that ozone might be a superior

563   indicator to NO_x for the photochemical process of isoprene under NO_x-dominant conditions. The

564   IEPOX-SOA tracers also correlated well with ozone ($r^2 = 0.36\text{-}0.70$) or O_x ($r^2 = 0.40\text{-}0.68$) in summer,

565   despite less strongly than HMML&/MAE-SOA species. –These observations clearly suggest that

566   atmospheric oxidation capacity (or the oxidation of isoprene to epoxide intermediates) plays a driving

567   role in summertime iSOA formation. In addition, weak to moderate ~~moderate~~ correlations ($r^2 = 0.23\text{-}$

568   0.45) were observed between the iSOA tracers and sulfate aerosol in 2019 and 2021, indicating that

569   sulfate aerosol also plays a role in controlling iSOA formation during these periods. In contrast,

570   wintertime iSOA species exhibited weak correlations with O_3 and O_x in all the three years (Figure 4d-

571   f). However, they all had moderate or strong correlations with sulfate aerosol ($r^2 = 0.36\text{-}0.68$) in 2015

572   and the iSOA OSs correlated ~~well~~ –moderately with sulfate ($r^2 = 0.35\text{-}0.58$) and LWC ($r^2 = 0.34\text{-}0.58$)

573   in 2019 and 2021. These results suggest that sulfate-mediated heterogeneous chemistry of isoprene

574   epoxide intermediates in aqueous aerosols is a key process controlling iSOA formation in winter (Surratt

575   et al., 2010; Yee et al., 2020; Lin et al., 2012). A sensitivity test considering the measurement

576   uncertainties of iSOA tracers did not significantly influence the correlation analysis results (see details

577   in Section S5).
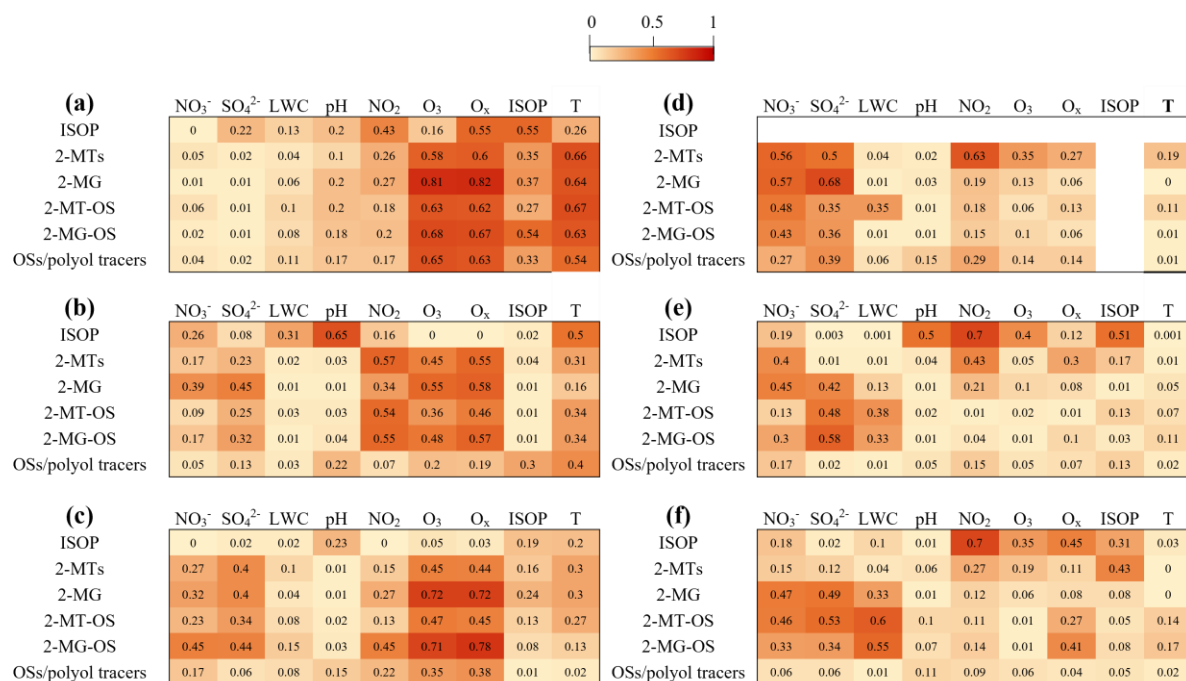
Figure 4. Coefficients of correlation (r^2) between iSOA compounds and various influencing factors of iSOA formation in (a-c) summer and (d-f) winter of 2015, 2019, and 2021, respectively. The ISOP is the abbreviation of isoprene.

As shown in Table S1, the concentrations of sulfate aerosol and LWC both decreased drastically over 2015-2021 ($p < 0.05$), which could explain the declining trend of iSOA in winter and partially contributed to the decreased formation of IEPOX-SOA in summer. Notably, the summertime average MDA8 (maximum daily 8-h average) O_3 concentration at the observation site increased from 2015 to 2017 and then decreased significantly in 2018, followed by a slight increasing trend between 2018 and 2021 (Figure ~~S5~~S6). This inter-annual trend of O_3 was similar to the trend of annual 90th percentile MDA8 O_3 concentration in the region of Shanghai (Figure ~~S5~~S6). As a result, the summertime average MDA8 O_3 concentration in 2015, 2019, and 2021 showed a slight downward trend. In addition, the simulated concentrations of OH radicals and ratios of (MVK+MACR)/isoprene both declined in 2019 compared to those in 2015 (see Table ~~S5~~S8), indicating a decline in the atmospheric oxidation capacity during the observation period. Similarly, the nighttime atmospheric oxidation capacity as indicated by the production rate of NO_3 radicals (PNO_3), calculated by multiplying the reaction rate coefficient between NO_2 and O_3 by their concentrations (Wang et al., 2023a), also decreased during this period (Figure ~~S6~~S7). The reduced atmospheric oxidation capacity further explained the decreased formation of ~~IEPOX-SOA~~iSOA OSs in summer during these years, but it could not explain the inter-annual

597 variation in summertime ~~HMML/MAE SOA~~2-MG and 2-MTs, suggesting that other factors might have

598 offset the anticipated decline in ~~HMML/MAE SOA~~these polyols during this period.

3.4 Heterogeneous reactivity of ambient aerosols

600  To better understand the role of heterogeneous chemistry in the formation and inter-annual

601 variations of iSOA, the reactive uptake coefficients (γ_{EPOXIDE}) of isoprene-derived epoxides on ambient

602 aerosols were estimated by a resistor model (eq. 4) (Xu et al., 2016; Pye et al., 2013). The pseudo-first-

603 order heterogeneous reaction rate constant (k_{het}, s^{-1}) of gas-phase IEPOX and HMML&/MAE could be

604 then estimated from γ_{EPOXIDE} via eq. 7. Currently, there are ~~four~~ five sets of reported third-order reaction

605 rate constants (i.e., $k_{\text{i,j}}$ in eq. 1) for the acid-catalyzed nucleophilic addition of water and sulfate to

606 IEPOX in the aqueous phase (Table 1). Piletic et al. (2013) predicted $k_{\text{i,j}}$ for IEPOX ($k_{\text{i,j-IEPOX}}^{-1}$) with a

607 computational model, which are two orders of magnitudes higher than the laboratory-measured values

608 ($k_{\text{i,j-IEPOX}}^{-2}$) by Riedel et al. (2015) and model-estimated values ($k_{\text{i,j-IEPOX}}^{-3}$) using CMAQ by Pye et al.

609 (2013). More recently, Pye et al. (2017) updated the values ($k_{\text{i,j-IEPOX}}^{-4}$) by constraining the $k_{\text{i,j-IEPOX}}^{-3}$

610 using measured 2-MT-OS/2-MTs in CMAQ and Chen et al. (2024) constrained reaction rate constant

611 of IEPOX ($k_{\text{i,j-IEPOX}}^{-5}$) using a phase-separation box model with chamber measurements. For HMML~~/~~

612 and MAE, there is a lack of direct measurements and theoretical calculations of their $k_{\text{i,j}}$ values. Pye et

613 al. (2013) assumed the same $k_{\text{i,j}}$ values as IEPOX with $k_{\text{i,H+}}$ of 9.0×10^{-4} M^{-2} s^{-1} for water and $2.0 \times$

614 10^{-4} M^{-2} s^{-1} for sulfate.

615

Table 1. Third-order reaction rate constants of IEPOX and HMML&/MAE with sulfate and water in the aqueous phase

	k_{i,H^+} (M^{-2}·s^{-1})		k_{i,HSO_4^-} (M^{-2}·s^{-1})		References
	i=H$_2$O	i=SO$_4^{2-}$	i=H$_2$O	i=SO$_4^{2-}$	
$k_{i,j\text{-IEPOX}}^{-1}$	5.3×10^{-2}	5.2×10^{-1}	—	—	(Piletic et al., 2013)
$k_{i,j\text{-IEPOX}}^{-2}$	3.4×10^{-4}	4.8×10^{-4}	—	—	(Riedel et al., 2015)
$k_{i,j\text{-IEPOX}}^{-3}$	9×10^{-4}	2×10^{-4}	1.3×10^{-5}	2.9×10^{-6}	(Pye et al., 2013)
$k_{i,j\text{-IEPOX}}^{-4}$	9×10^{-4}	8.8×10^{-3}	1.3×10^{-5}	2.9×10^{-6}	(Pye et al., 2017)
$k_{i,j\text{-IEPOX}}^{-5}$	5.3×10^{-4}	5.2×10^{-3}	—	—	(Chen et al., 2024)
$k_{i,j\text{-HMML&/MAE}}$	9×10^{-4}	2×10^{-4}	1.3×10^{-5}	2.9×10^{-6}	(Pye et al., 2013)
~~$k_{i,j\text{-HMML/MAE}}^{-1}$~~	~~9×10^{-4}~~	~~2×10^{-3}~~	~~1.3×10^{-5}~~	~~2.9×10^{-6}~~	—
~~$k_{i,j\text{-HMML/MAE}}^{-2}$~~	~~9×10^{-4}~~	~~2×10^{-2}~~	~~1.3×10^{-5}~~	~~2.9×10^{-6}~~	—

Firstly, the $k_{i,j}$ values of IEPOX and HMML&/MAE were evaluated by comparing the measured ratios of 2-MT-OS/2-MTs and 2-MG-OS/2-MG with the calculated ratios of the pseudo-first-order rate constants for the nucleophilic addition reactions of epoxides with sulfate and water ($k_{aq,\,SO_4^{2-}}/k_{aq,\,H_2O}$).

The results are shown in Figure ~~S7~~ S8 and ~~S8~~ S9. For IEPOX, the $k_{aq,\,SO_4^{2-}}/k_{aq,\,H_2O}$ ratios were close to measured particulate ratios of 2-MT-OS/2-MTs when using $k_{i,j\text{-IEPOX}}^{-1}$~~,~~ ~~and~~ $k_{i,j\text{-IEPOX}}^{-4}$, and $k_{i,j\text{-IEPOX}}^{-5}$ suggested by Piletic et al. (2013)~~ and,~~ Pye et al. (2017), and Chen et al. (2024), respectively (Figure S8). However, when taking into account the underestimation of 2-MT-OS due to matrix effect, all estimated ratios were lower than the measured values. ~~That was still the case when taking into account the quantification uncertainties and the gas-phase fractions of 2-MT-OS and 2-MTs.~~ Similarly,~~However,~~ the calculated $k_{aq,\,SO_4^{2-}}/k_{aq,\,H_2O}$ ratios for HMML and MAE were 1-2 orders of magnitude lower than the measured 2-MG-OS/2-MG ratios (Figure ~~S7~~S9) and such a discrepancy would be larger when considering the matrix effect of 2-MG-OS. This result indicates that the k_{ij} of isoprene-derived epoxides, particularly that of HMML and MAE,~~HMML/MAE~~ with sulfate was likely underestimated, since Pye et al. (2013) found their hydrolysis rate constant ~~of HMML/MAE could lead to~~allowed a good prediction of the concentration of 2-MG. ~~Therefore, the $k_{i,j}$ of HMML/MAE with sulfate was elevated by one ($k_{i,j\text{-HMML}}^{-1}$) to two ($k_{i,j\text{-HMML}}^{-2}$) orders of magnitude to estimate the k_{het} of HMML/MAE.~~

634   Figure 5 shows the γ and k_{het} values for IEPOX and HMML~~&~~~~/~~MAE estimated using different sets

635   of kinetic parameters listed in Table 1. The CMAQ-modeled values are also displayed for comparison.

636   ~~The value of k_{het} for HMML/MAE calculated by elevated $k_{\text{i,j-HMML}}^{-1}$ and $k_{\text{i,j-HMML}}^{-2}$ increased by about~~

637   ~~one and two folds (shown in Figure 5c), respectively. However, the inter-annual trend of $k_{\text{het-HMML}}$ was~~

638   ~~unaltered. In addition, the~~ The k_{het} estimated by $\underline{k_{i,\text{j-IEPOX}}^{-1}, k_{i,\text{j-IEPOX}}^{-2}}$ and $\underline{k_{i,\text{j-IEPOX}}^{-5}}$~~$k_{i,\text{j-IEPOX}}^{-1}$ and $k_{i,\text{j-IEPOX}}^{-}$~~

639   ~~^{2}~~ in summer had highest values in 2019. This might be attributed to the fact that these ~~two~~ three sets of

640   parameters lack the third-order reaction rate constant of IEPOX with nucleophiles catalyzed by bisulfate

641   (Table 1). As a comparison, we calculated the k_{het} of IEPOX and HMML~~&~~~~/~~MAE excluding the reaction

642   rate constant catalyzed by bisulfate using $\underline{k_{\text{i,j-IEPOX}}^{-3}}$ and $\underline{k_{\text{i,j-IEPOX}}^{-4}}$ (Figure ~~S9~~S10). We found that the

643   inter-annual trend of IEPOX (Figure ~~S9a~~S10a) and HMML~~/~~&MAE (Figure ~~S9b~~S10b) in summer~~time~~

644   was altered and similar to that of IEPOX calculated by $\underline{k_{\text{i,j-IEPOX}}^{-1}, k_{\text{i,j-IEPOX}}^{-2}}$ and $\underline{k_{\text{i,j-IEPOX}}^{-5}}$~~$k_{\text{i,j-IEPOX}}^{-1}$ and~~

645   ~~$k_{\text{i,j-IEPOX}}^{-2}$~~ $\underline{,}$ ~~w~~While the inter-annual trend of k_{het} in winter was not sensitive to the exclusion of reaction

646   rate constant catalyzed by bisulfate. This result indicates a contribution of nucleophilic-addition of

647   epoxides catalyzed by bisulfate to the heterogeneous reactivity. $\underline{\text{It also suggests that the } k_{\text{i,j-IEPOX}}^{-4} \text{ is}}$

648    $\underline{\text{more appropriate for predicting aerosol heterogeneous reactivity toward IEPOX than other four sets of}}$

649    $\underline{\text{kinetic parameters.}}$~~It is also proved that the $k_{\text{i,j-IEPOX}}^{-4}$ is more appreciate for predicting the measured~~

650   ~~ratios of 2-MT-OS to 2-MTs and the aerosol heterogeneous reactivity toward IEPOX.~~

651
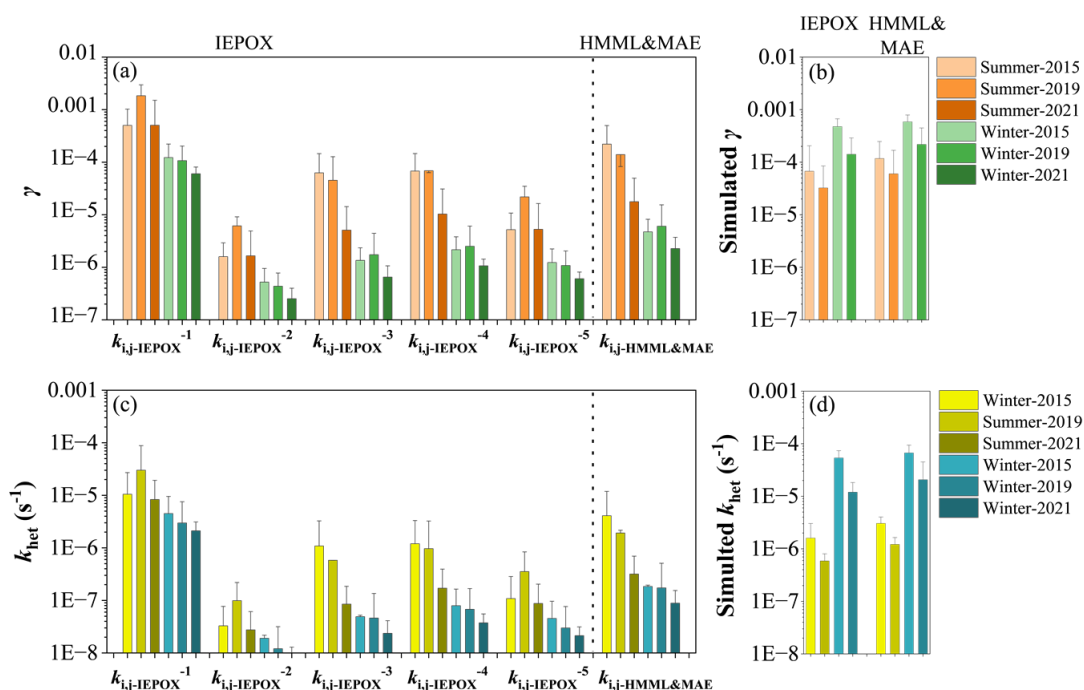
Figure 5. Reactive uptake coefficients (γ) and pseudo-first-order heterogeneous reaction rate constant (k_{het}, s^{-1}) of gas-phase IEPOX and HMML~~/~~&MAE estimated using different sets of $k_{i,j\text{-IEPOX}}$ and $k_{i,j\text{-HMML}\&\text{MAE}}$ listed in Table 1 (a and c) and simulated by CMAQ model in Case 1 (b and d).

As shown in Figure 5a and 5c, the estimated γ and k_{het} of IEPOX and HMML~~/~~&MAE using $k_{i,j\text{-IEPOX}}^{-4}$ and ~~,~~ $k_{i,j\text{-HMML\&MAE}}$~~$_{\text{HMML}}^{-1}$, and $k_{i,j\text{-HMML}}^{-2}$~~ showed a similar trend which decreased in both winter and summer. Similar decreasing trends in γ and k_{het} were also simulated by CMAQ (Figure 5b and 5d). The calculated γ and k_{het} values of IEPOX and HMML&~~/~~MAE in summer using $k_{i,j\text{-IEPOX}}^{-4}$ and $k_{i,j\text{-HMML\&MAE}}$~~HMML~~, respectively, are consistent with the simulated results, while the calculated values in winter were significantly lower than the simulations, which is likely attributed to the significantly under-predicted aerosol pH and thereby over-predicted aerosol reactivity in winter by the model. Overall, the declining trend of both calculated and model-predicted k_{het} offers an explanation for the decreasing trend of ~~iSOA in both seasons and IEPOX SOA~~2-MT-OS and 2-MG-OS in summer, but it could not explain the observed trend of 2-MG and 2-MTs ~~HMML/MAE SOA~~ in summer.

3.5 Meteorological influences on iSOA variation

As discussed above, the variations in chemical factors (including atmospheric oxidizing capacity and aerosol heterogeneous reactivity) could well explain the declining trend of both summertime and wintertime ~~IEPOX SOA and wintertime HMML/MAE SOA~~iSOA OSs, but not the trend of summertime ~~HMML/MAE SOA~~2-MG and 2-MTs during the period of 2015-2021. Since meteorological conditions could exert a significant influence on the concentrations of atmospheric pollutants (Liu et al., 2023b; Gu et al., 2023), we further investigate the impact of the variation in meteorological conditions on the variation of iSOA during the observation period.

To do so, the CMAQ simulations for 2019 adopted the emissions of 2015 (Test Case), so the variations in simulated iSOA concentration from 2015 to 2019 in this case is mainly attributed to the changes in the meteorological conditions during these years. As shown in Figure 6, the simulated variations in median concentrations of 2-MTs, 2-MT-OS, 2-MG, and 2-MG-OS in the Test case accounted for 38.3-82.4% and 66.5-99.2% of the concentration reductions in Case 1 in summer and winter, respectively. ~~in 2019 decreased by 45.7%, 85.9%, 57.0%, and 70.9% in summer and 61.2 %, 38.4%, 53.2%, and 75.6% in winter, respectively, compared to the concentrations in 2015 in the Test~~

680 ~~Case. Such decreases were close to the concentration reductions simulated in the Case 1,~~ This

681 suggest~~sing~~ that the alteration in meteorological conditions exerts a more substantial influence on the

682 variation in iSOA concentrations compared to the changes in emissions.

683

684
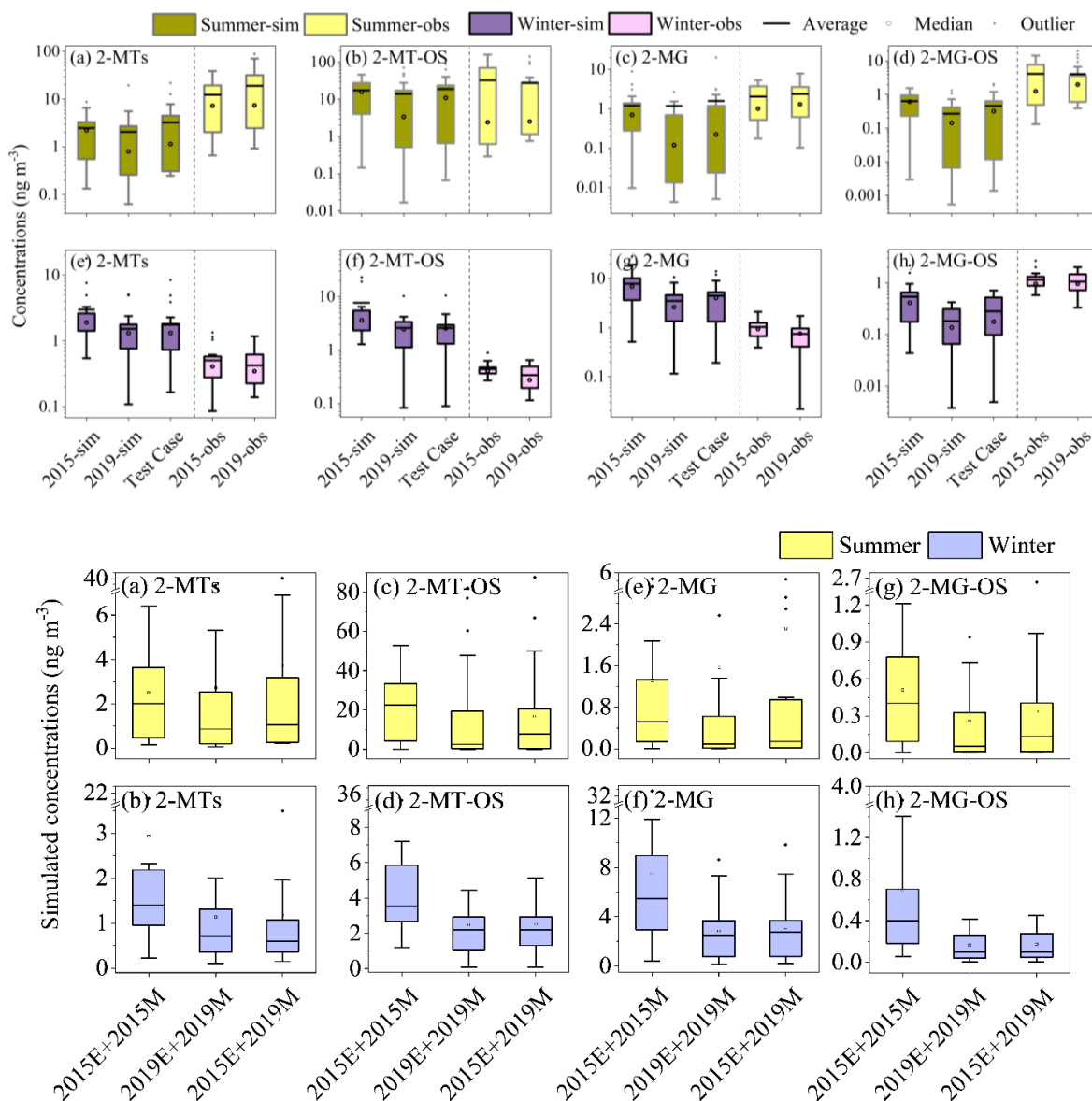
685 Figure 6. Simulated concentrations of 2-MTs, 2-MT-OS, 2-MG and 2-MG-OS in summer (a-d~~a, c, e~~

686 ~~and g~~) and winter (~~b, d, f and h~~e-h) in Case 1 (2015-sim and 2019-sim) ~~(2015E+2015M vs.~~

687 ~~2019E+2019M)~~ and Test Case (simulations with 2015 emissions and 2019 meteorological conditions).

688 The observed concentrations of 2-MTs, 2-MT-OS, 2-MG, and 2-MG-OS in 2015 and 2019 are also

689 displayed (Detailed model-measurement comparisons are provided in Section 3.2; after accounting for

690 matrix effect, 2-MT-OS would decrease more sharply and 2-MG-OS would show a descending inter-

691 annual trend, consistent with model simulations). ~~(2015E+2015M vs. 2015E+2019M).~~

692   It should be noted that the variations in meteorological conditions not only affect the physical

693   processes such as dilution and transport, but also influence the chemical processes determining the

694   formation of iSOA. To investigate the impacts of physical and chemical factors associated with the

695   variations in meteorological conditions on the abundance of iSOA, the concentrations of elemental

696   carbon (EC) were simulated in the Test Case. As shown in Figure 7, the simulated ~~average~~ median

697   concentrations of summertime and wintertime EC in 2019 both decreased by ~~15.9~~32.8% ~~and 22.1%~~,

698   respectively, compared to those in 2015. Since EC is a primary pollutant and chemically inert under

699   atmospheric conditions, the variations in its concentration in the Test Case is attributed to the changes

700   in the physical processes, contributing approximately 59.5% of the EC reductions between 2015 and

701   2019 (Case 1). As a result, we could expect a similar contribution of the physical processes to the

702   reduction in iSOA concentration ~~(15.9% in summer and 22.1% in winter)~~. Notably, such reductions are

703   significantly smaller than the simulated concentration reductions of iSOA in the Test case (Figure 6),

704   suggesting that the chemical factors associated with the changes in meteorological conditions play a

705   crucial role in determining the trend of iSOA in Shanghai, consistent with the above analysis based on

706   the observations. However, we note that the alternation in meteorological conditions cannot explain the

707   observed non-declining trend of ~~HMML/MAE-SOA~~2-MG and 2-MTs in summer, implying that some

708   other factors that are not well represented in the CMAQ model may play a role in controlling such a

709   trend.

710

711
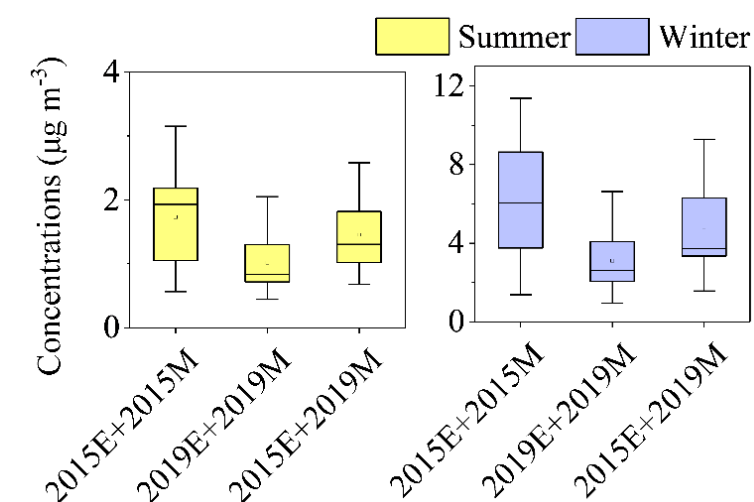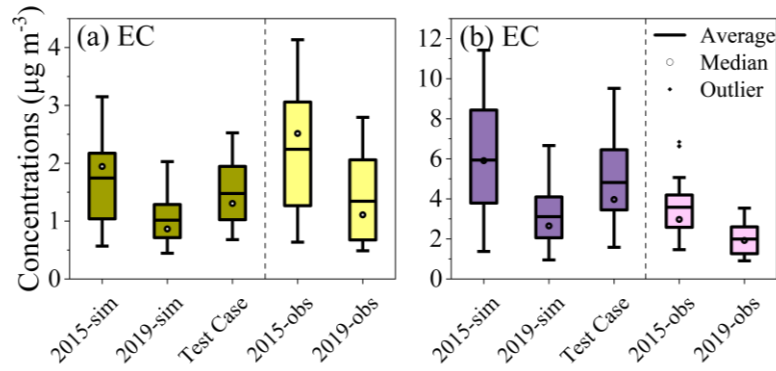
712 Figure 7. Simulated EC concentrations in Case 1 (2015-sim and 2019-sim~~2015E+2015M vs.~~

713 ~~2019E+2019M~~) and Test Case (simulations with 2015 emissions and 2019 meteorological

714 conditions~~2015E+2015M vs. 2015E+2019M~~) in (a) summer and (b) winter. The measured

715 concentrations are also displayed and their trend is consistent with the simulations.

716   As discussed in Section 3.2, there is a large contribution of non-IEPOX sources to 2-MTs. Such

717 sources might not be well represented in the model, which could explain the discrepancy between the

718 simulated and observed trend of 2-MTs in summer. On the other hand, MACR is known as a first-

719 generation oxidation product of isoprene and an important intermediate for iSOA formation through

720 NOx-dominant pathways (Nguyen et al., 2015), but it can also originate from ~~As the precursor to~~

721 ~~HMML and MAE, the MACR can be derived from both~~ primary sources, such as biological emissions

722 (Jardine et al., 2012), residential wood burning (Gaeggeler et al., 2008), and vehicle exhaust emissions

723 (He et al., 2009)~~, and secondary formation from gas-phase oxidation of isoprene~~ (Schwantes et al., 2015;

724 Surratt et al., 2010). ~~Field studies have demonstrated that the concentration of MACR in urban areas~~

725 ~~was predominantly influenced by vehicle emissions~~ (Ling et al., 2019b; Park et al., 2011). In certain

726 urban areas, MACR arises primarily from vehicular emissions, as observed at the Heshan site in the

727 Pearl River Delta region, China (Ling et al., 2019a)~~,~~ and in Houston, US (Park et al., 2011). In the

728 present work, the simulated MACR concentration demonstrated a decreasing trend from 2015 to 2019

729 in summer when the contribution of primary emissions was considered in the model. Yet, our recent

730 study revealed that, despite a good agreement between modelled and measured isoprene concentrations,

731 the model under-predicted the peak concentrations of MACR during the noon in urban Shanghai (Li et

732 al., 2022), implying an underestimation of secondary formation and/or primary emissions of MACR in

733 the model. Furthermore, Gu et al. (2023) reported that in the southern cities of Jiangsu Province, which

734 is adjacent to Shanghai, anthropogenic VOCs increased by approximately 15% from 2015 to 2019.

735 Therefore, we infer that the sources (e.g., primary emissions) of MACR might be ~~underappreciated~~

736 under-predicted in this work, which may provide a rationale for ~~the under-prediction of HMML/MAE~~

737 ~~SOA concentrations and~~ the inconsistency between ~~its~~ simulated and observed inter-annual trends of 2-

738 MG.

4. Conclusions

740 In this study, ~~three-year measurements~~observations of isoprene-derived SOA species in ambient

741 $PM_{2.5}$ were conducted at an urban site in Shanghai, China ~~during the period of 2015-2021~~ during

742 summers and winters in 2015, 2019, and 2021, aiming to understand the response of biogenic SOA

743 formation to anthropogenic emission reductions in polluted regions. The complementary CMAQ model

744 simulations were also performed for 2015 and 2019 and the results are compared to the measurements.

745 It is found that the particulate concentration of total iSOA tracers, dominated by IEPOX-SOA species

746 including 2-MT-OS and 2-MT, had a decreasing trend from 2015 to 2021 (55.6, 51.0, and 29.7 ng m^{-3}

747 in 2015, 2019, and 2021, respectively)~~.~~, ~~with a dominant contribution from IEPOX-SOA species (52.6,~~

748 ~~46.7, and 25.8 ng m^{-3} in 2015, 2019, and 2021, respectively), while HMML/MAE SOA species (4.3,~~

749 ~~4.2, and 4.3 ng m^{-3} in 2015, 2019, and 2021, respectively)~~When the measurement uncertainties of iSOA

750 tracers such as the matrix effect of OSs were considered, 2-MT-OS and 2-MG-OS exhibited a declining

751 trend in both seasons during the observation period. In contrast, 2-MG and 2-MTs showed no significant

752 inter-annual variations ~~did not decrease significantly and, a~~After accounting for ~~their~~ the gas-phase

753 fraction, 2-MG even exhibited a slight upward trend in summer during these years.

754 The isoprene-derived SOA species correlated well with ozone and O_x in summer but with sulfate

755 in winter, suggesting that the atmospheric oxidation of isoprene to epoxide intermediates and their

756 subsequent reactive uptake on aqueous aerosols are the key steps driving the formation of iSOA in

757 summer and winter, respectively. ~~The O$_3$ and Ox-represented atmospheric oxidizing capacity as well as~~

758 ~~the kinetically estimated aerosol heterogeneous reactivity decreased significantly during the observation~~

759 ~~period~~ The Ox-represented atmospheric oxidizing capacity and aerosol heterogeneous reactivity

760 decreased significantly during the observation period, which provided an explanation for the decreasing

trend of ~~IEPOX-SOA and wintertime HMML/MAE-SOA~~iSOA tracers in summer and winter (with the

exception of ~~, but not the~~ summertime ~~HMML/MAE-SOA~~2-MG and 2-MTs).

    The CMAQ model predicted the ~~levels~~ concentrations of iSOA tracers reasonably well and

captured the declining trend of total iSOA, 2-MT-OS, and 2-MG-OS ~~measured IEPOX-SOA~~ in both

seasons ~~and HMML/MAE-SOA in winter. However, the predicted declining trend of HMML/MAE-~~

~~SOA,~~ but not the insignificant inter-annual variations of 2-MG and 2-MTs in summer ~~in summer was~~

~~contrary to the observed trend.~~ Further model simulations show that inter-annual variations in iSOA

concentration are mainly governed by the changes in the meteorological conditions rather than the

emissions. Consistent with the analysis based on the observation data, the model simulations show that

the changes in chemical factors such as aerosol heterogeneous reactivity caused by variations in

meteorological conditions play an important role in controlling the inter-annual trend of iSOA. The

discrepancy between measured and modeled inter-annual trends of 2-MG and 2-MTs is likely ascribed

to the presence of unaccounted or underrepresented factors such as the direct emissions of MACR and

2-MTs in the model. ~~The model results also suggest the presence of unaccounted or underrepresented~~

~~factors such as the direct emissions of MACR in the model, which led to the discrepancy between the~~

~~modeled and observed trends of HMML/MAE-SOA in summer.~~ Overall, our study revealed the

responses and underlying driving factors of iSOA formation under rapidly changing anthropogenic

emissions conditions in a typical Chinese ~~megacities~~megacity. It also highlights the importance of

tailored emission reductions for the mitigation of PM formation from biogenic emissions through

~~regulating chemical factors such as~~ the regulation of atmospheric oxidizing capacity and aerosol

chemical reactivity ~~in the mitigation of the PM pollution from biogenic emissions~~.

Data availability.

The data presented in this work are available upon request from the corresponding author.

Competing interests.

The authors declare no competing interest relevant to this study.

Author Contributions.

787 YZ conceived and designed the study, HH, YW, and TY performed the field observation and analyzed

788 the data, JL, YL, TL, and YS performed the model simulations, HH, YZ, and JL wrote the paper, and

789 all other authors contributed to the discussion and writing.

790 **Acknowledgements.**

791 This study was supported by the National Key R&D Program of China (no. 2022YFC3701003) and the

792 National Natural Science Foundation of China (no. 22376137 and 22206120).

793 **References**

794 Bates, K. H., Crounse, J. D., St. Clair, J. M., Bennett, N. B., Nguyen, T. B., Seinfeld, J. H., Stoltz, B. M., and
795   Wennberg, P. O.: Gas Phase Production and Loss of Isoprene Epoxydiols, J. Phys. Chem. A, 118, 1237-
796   1246, 10.1021/jp4107958, 2014.

797 Bryant, D. J., Elzein, A., Newland, M., White, E., Swift, S., Watkins, A., Deng, W., Song, W., Wang, S.,
798   Zhang, Y., Wang, X., Rickard, A. R., and Hamilton, J. F.: Importance of Oxidants and Temperature in the
799   Formation of Biogenic Organosulfates and Nitrooxy Organosulfates, ACS Earth Space Chem., 5, 2291-
800   2306, 10.1021/acsearthspacechem.1c00204, 2021.

801 Bryant, D. J., Dixon, W. J., Hopkins, J. R., Dunmore, R. E., Pereira, K. L., Shaw, M., Squires, F. A., Bannan,
802   T. J., Mehra, A., Worrall, S. D., Bacak, A., Coe, H., Percival, C. J., Whalley, L. K., Heard, D. E., Slater, E.
803   J., Ouyang, B., Cui, T., Surratt, J. D., Liu, D., Shi, Z., Harrison, R., Sun, Y., Xu, W., Lewis, A. C., Lee, J.
804   D., Rickard, A. R., and Hamilton, J. F.: Strong anthropogenic control of secondary organic aerosol
805   formation from isoprene in Beijing, Atmos. Chem. Phys., 20, 7531-7552, 10.5194/acp-20-7531-2020,
806   2020.

807 Budisulistiorini, S. H., Li, X., Bairai, S. T., Renfro, J., Liu, Y., Liu, Y. J., McKinney, K. A., Martin, S. T.,
808   McNeill, V. F., Pye, H. O. T., Nenes, A., Neff, M. E., Stone, E. A., Mueller, S., Knote, C., Shaw, S. L.,
809   Zhang, Z., Gold, A., and Surratt, J. D.: Examining the effects of anthropogenic emissions on isoprene-
810   derived secondary organic aerosol formation during the 2013 Southern Oxidant and Aerosol Study (SOAS)
811   at the Look Rock, Tennessee ground site, Atmos. Chem. Phys., 15, 8871-8888, 10.5194/acp-15-8871-
812   2015, 2015.

813 Chen, Y., Ng, A. E., Green, J., Zhang, Y., Riva, M., Riedel, T. P., Pye, H. O. T., Lei, Z., Olson, N. E., Cooke,
814   M. E., Zhang, Z., Vizuete, W., Gold, A., Turpin, B. J., Ault, A. P., and Surratt, J. D.: Applying a Phase-
815   Separation Parameterization in Modeling Secondary Organic Aerosol Formation from Acid-Driven
816   Reactive Uptake of Isoprene Epoxydiols under Humid Conditions, ACS ES&T Air, 1, 511-524,
817   10.1021/acsestair.4c00002, 2024.

818 Cui, T., Zeng, Z., dos Santos, E. O., Zhang, Z., Chen, Y., Zhang, Y., Rose, C. A., Budisulistiorini, S. H.,
819   Collins, L. B., Bodnar, W. M., de Souza, R. A. F., Martin, S. T., Machado, C. M. D., Turpin, B. J., Gold,
820   A., Ault, A. P., and Surratt, J. D.: Development of a hydrophilic interaction liquid chromatography (HILIC)
821   method for the chemical characterization of water-soluble isoprene epoxydiol (IEPOX)-derived secondary
822   organic aerosol, ~~ENVIRON SCI-PROC IMP~~Environ. Sci. Proc. Imp., 20, 1524-1536,
823   10.1039/C8EM00308D, 2018.

824 Ding, X., He, Q. F., Shen, R. Q., Yu, Q. Q., and Wang, X. M.: Spatial distributions of secondary organic
825   aerosols from isoprene, monoterpenes, beta-caryophyllene, and aromatics over China during summer, J.
826   Geophys. Res. ~~atmos~~Atmos., 119, 11877-11891, Doi 10.1002/2014jd021748, 2014.

827 Eddingsaas, N. C., VanderVelde, D. G., and Wennberg, P. O.: Kinetics and Products of the Acid-Catalyzed
828   Ring-Opening of Atmospherically Relevant Butyl Epoxy Alcohols, J. Phys. Chem. A, 114, 8106-8113,
829   10.1021/jp103907c, 2010.

Fan, Y., Liu, C.-Q., Li, L., Ren, L., Ren, H., Zhang, Z., Li, Q., Wang, S., Hu, W., Deng, J., Wu, L., Zhong, S., Zhao, Y., Pavuluri, C. M., Li, X., Pan, X., Sun, Y., Wang, Z., Kawamura, K., Shi, Z., and Fu, P.: Large contributions of biogenic and anthropogenic sources to fine organic aerosols in Tianjin, North China, Atmos. Chem. Phys., 20, 117-137, 10.5194/acp-20-117-2020, 2020.

Frauenheim, M., Offenberg, J., Zhang, Z., Surratt, J. D., and Gold, A.: The C5–Alkene Triol Conundrum: Structural Characterization and Quantitation of Isoprene-Derived C5H10O3 Reactive Uptake Products, Environ. Sci. Technol. Lett, 9, 829-836, 10.1021/acs.estlett.2c00548, 2022.

Frauenheim, M., Offenberg, J., Zhang, Z., Surratt, J. D., and Gold, A.: Chemical Composition of Secondary Organic Aerosol Formed from the Oxidation of Semivolatile Isoprene Epoxydiol Isomerization Products, Environ. Sci. Technol, 58, 22571-22582, 10.1021/acs.est.4c06850, 2024.

Fu, P., Aggarwal, S. G., Chen, J., Li, J., Sun, Y., Wang, Z., Chen, H., Liao, H., Ding, A., Umarji, G. S., Patil, R. S., Chen, Q., and Kawamura, K.: Molecular Markers of Secondary Organic Aerosol in Mumbai, India, Environ Sci Technol, 50, 4659-4667, 10.1021/acs.est.6b00372, 2016.

Fu, P. Q., Kawamura, K., Chen, J., and Miyazaki, Y.: Secondary Production of Organic Aerosols from Biogenic VOCs over Mt. Fuji, Japan, Environ Sci Technol, 48, 8491-8497, 10.1021/es500794d, 2014.

Fu, P. Q., Kawamura, K., Chen, J., Li, J., Sun, Y. L., Liu, Y., Tachibana, E., Aggarwal, S. G., Okuzawa, K., Tanimoto, H., Kanaya, Y., and Wang, Z. F.: Diurnal variations of organic molecular tracers and stable carbon isotopic composition in atmospheric aerosols over Mt. Tai in the North China Plain: an influence of biomass burning, Atmos. Chem. Phys., 12, 8359-8375, 10.5194/acp-12-8359-2012, 2012.

Gaeggeler, K., Prevot, A. S. H., Dommen, J., Legreid, G., Reimann, S., and Baltensperger, U.: Residential wood burning in an Alpine valley as a source for oxygenated volatile organic compounds, hydrocarbons and organic acids, Atmos. Environ, 42, 8278-8287, 10.1016/j.atmosenv.2008.07.038, 2008.

Geng, G., Liu, Y., Liu, Y., Liu, S., Cheng, J., Yan, L., Wu, N., Hu, H., Tong, D., Zheng, B., Yin, Z., He, K., and Zhang, Q.: Efficacy of China's clean air actions to tackle PM2.5 pollution between 2013 and 2020, Nat. Geosci, 17, 987-994, 10.1038/s41561-024-01540-z, 2024.

Gong, J., Yin, Z., Lei, Y., Lu, X., Zhang, Q., Cai, C., Chai, Q., Chen, H., Chen, R., Chen, W., Cheng, J., Chi, X., Dai, H., Dong, Z., Geng, G., Hu, J., Hu, S., Huang, C., Li, T., Li, W., Li, X., Lin, Y., Liu, J., Ma, J., Qin, Y., Tang, W., Tong, D., Wang, J., Wang, L., Wang, Q., Wang, X., Wang, X., Wu, L., Wu, R., Xiao, Q., Xie, Y., Xu, X., Xue, T., Yu, H., Zhang, D., Zhang, L., Zhang, N., Zhang, S., Zhang, S., Zhang, X., Zhang, Z., Zhao, H., Zheng, B., Zheng, Y., Zhu, T., Wang, H., Wang, J., and He, K.: The 2023 report of the synergetic roadmap on carbon neutrality and clean air for China: Carbon reduction, pollution mitigation, greening, and growth, Environ. Sci. Ecotechnol., 23, 100517, https://doi.org/10.1016/j.ese.2024.100517, 2025.

Gu, C., Zhang, L., Xu, Z., Xia, S., Wang, Y., Li, L., Wang, Z., Zhao, Q., Wang, H., and Zhao, Y.: High-resolution regional emission inventory contributes to the evaluation of policy effectiveness: a case study in Jiangsu Province, China, Atmos. Chem. Phys., 23, 4247-4269, 10.5194/acp-23-4247-2023, 2023.

Guenther, A., Karl, T., Harley, P., Wiedinmyer, C., Palmer, P. I., and Geron, C.: Estimates of global terrestrial isoprene emissions using MEGAN (Model of Emissions of Gases and Aerosols from Nature), Atmos. Chem. Phys., 6, 3181-3210, 10.5194/acp-6-3181-2006, 2006.

Guo, H., Xu, L., Bougiatioti, A., Cerully, K. M., Capps, S. L., Hite Jr, J. R., Carlton, A. G., Lee, S. H., Bergin, M. H., Ng, N. L., Nenes, A., and Weber, R. J.: Fine-particle water and pH in the southeastern United States, Atmos. Chem. Phys., 15, 5211-5228, 10.5194/acp-15-5211-2015, 2015.

He, C., Ge, Y. S., Tan, J. W., You, K. W., Han, X. K., Wang, J. F., You, Q. W., and Shah, A. N.: Comparison of carbonyl compounds emissions from diesel engine fueled with biodiesel and diesel, Atmos. Environ, 43, 3657-3661, 10.1016/j.atmosenv.2009.04.007, 2009.

He, Q.-F., Ding, X., Fu, X.-X., Zhang, Y.-Q., Wang, J.-Q., Liu, Y.-X., Tang, M.-J., Wang, X.-M., and Rudich, Y.: Secondary Organic Aerosol Formation From Isoprene Epoxides in the Pearl River Delta, South China: IEPOX- and HMML-Derived Tracers, J Geophys Res-atmos, 123, 6999-7012, 10.1029/2017jd028242, 2018.

He, Q.-F., Ding, X., Wang, X.-M., Yu, J.-Z., Fu, X.-X., Liu, T.-Y., Zhang, Z., Xue, J., Chen, D.-H., Zhong, L.-J., and Donahue, N. M.: Organosulfates from Pinene and Isoprene over the Pearl River Delta, South

China: Seasonal Variation and Implication in Formation Mechanisms, Environ Sci Technol, 48, 9236-9245, 10.1021/es501299v, 2014.

Heald, C. L., Henze, D. K., Horowitz, L. W., Feddema, J., Lamarque, J. F., Guenther, A., Hess, P. G., Vitt, F., Seinfeld, J. H., Goldstein, A. H., and Fung, I.: Predicted change in global secondary organic aerosol concentrations in response to future climate, emissions, and land use change, J. Geophys. Res.-atmos., 113, 10.1029/2007jd009092, 2008.

Hennigan, C. J., Izumi, J., Sullivan, A. P., Weber, R. J., and Nenes, A.: A critical evaluation of proxy methods used to estimate the acidity of atmospheric particles, Atmos. Chem. Phys., 15, 2775-2790, 10.5194/acp-15-2775-2015, 2015.

Hettiyadura, A. P. S., Al-Naiema, I. M., Hughes, D. D., Fang, T., and Stone, E. A.: Organosulfates in Atlanta, Georgia: anthropogenic influences on biogenic secondary organic aerosol formation, Atmos. Chem. Phys., 19, 3191-3206, 10.5194/acp-19-3191-2019, 2019.

Hettiyadura, A. P. S., Stone, E. A., Kundu, S., Baker, Z., Geddes, E., Richards, K., and Humphry, T.: Determination of atmospheric organosulfates using HILIC chromatography with MS detection, Atmos. Meas. Tech., 8, 2347-2358, 10.5194/amt-8-2347-2015, 2015.

Hu, D., Bian, Q., Li, T. W. Y., Lau, A. K. H., and Yu, J. Z.: Contributions of isoprene, monoterpenes, β-caryophyllene, and toluene to secondary organic aerosols in Hong Kong during the summer of 2006, J Geophys Res-atmos, 113, https://doi.org/10.1029/2008JD010437, 2008.

Isaacman-VanWertz, G., Yee, L. D., Kreisberg, N. M., Wernis, R., Moss, J. A., Hering, S. V., de Sá, S. S., Martin, S. T., Alexander, M. L., Palm, B. B., Hu, W., Campuzano-Jost, P., Day, D. A., Jimenez, J. L., Riva, M., Surratt, J. D., Viegas, J., Manzi, A., Edgerton, E., Baumann, K., Souza, R., Artaxo, P., and Goldstein, A. H.: Ambient Gas-Particle Partitioning of Tracers for Biogenic Oxidation, Environ. Sci. Technol., 50, 9952-9962, 10.1021/acs.est.6b01674, 2016.

Jardine, K. J., Monson, R. K., Abrell, L., Saleska, S. R., Arneth, A., Jardine, A., Ishida, F. Y., Serrano, A. M. Y., Artaxo, P., Karl, T., Fares, S., Goldstein, A., Loreto, F., and Huxman, T.: Within-plant isoprene oxidation confirmed by direct emissions of oxidation products methyl vinyl ketone and methacrolein, Global Change Biol. , 18, 973-984, 10.1111/j.1365-2486.2011.02610.x, 2012.

Kang, M. J., Fu, P. Q., Kawamura, K., Yang, F., Zhang, H. L., Zang, Z. C., Ren, H., Ren, L. J., Zhao, Y., Sun, Y. L., and Wang, Z. F.: Characterization of biogenic primary and secondary organic aerosols in the marine atmosphere over the East China Sea, Atmos. Chem. Phys., 18, 13947-13967, 10.5194/acp-18-13947-2018, 2018.

Kebarle, P.: A brief overview of the present status of the mechanisms involved in electrospray mass spectrometry, J Mass. Spectrom., 35, 804-817, 10.1002/1096-9888(200007)35:7<804::Aid-jms22>3.0.Co;2-q, 2000.

Kelly, J. M., Doherty, R. M., O'Connor, F. M., and Mann, G. W.: The impact of biogenic, anthropogenic, and biomass burning volatile organic compound emissions on regional and seasonal variations in secondary organic aerosol, Atmos. Chem. Phys., 18, 7393-7422, 10.5194/acp-18-7393-2018, 2018.

Kjaergaard, H. G., Knap, H. C., Ørnsø, K. B., Jørgensen, S., Crounse, J. D., Paulot, F., and Wennberg, P. O.: Atmospheric fate of methacrolein. 2. Formation of lactone and implications for organic aerosol production, J. Phys. Chem. A, 116, 5763-5768, 10.1021/jp210853h, 2012.

Kurokawa, J. and Ohara, T.: Long-term historical trends in air pollutant emissions in Asia: Regional Emission inventory in ASia (REAS) version 3, Atmos. Chem. Phys., 20, 12761-12793, 10.5194/acp-20-12761-2020, 2020.

Lewandowski, M., Piletic, I. R., Kleindienst, T. E., Offenberg, J. H., Beaver, M. R., Jaoui, M., Docherty, K. S., and Edney, E. O.: Secondary organic aerosol characterisation at field sites across the United States during the spring–summer period, Int. J. Environ. Anal. Chem., 93, 1084-1103, 10.1080/03067319.2013.803545, 2013.

Li, J., Xie, X., Li, L., Wang, X., Wang, H., Jing, S. a., Ying, Q., Qin, M., and Hu, J.: Fate of Oxygenated Volatile Organic Compounds in the Yangtze River Delta Region: Source Contributions and Impacts on the Atmospheric Oxidation Capacity, Environ. Sci. Technol., 56, 11212-11224, 10.1021/acs.est.2c00038, 2022.

Lin, Y. H., Knipping, E. M., Edgerton, E. S., Shaw, S. L., and Surratt, J. D.: Investigating the influences of SO_2 and NH_3 levels on isoprene-derived secondary organic aerosol formation using conditional sampling approaches, Atmos. Chem. Phys., 13, 8457-8470, 10.5194/acp-13-8457-2013, 2013a.

Lin, Y. H., Zhang, H., Pye, H. O. T., Zhang, Z., Marth, W. J., Park, S., Arashiro, M., Cui, T., Budisulistiorini, S. H., and Sexton, K. G.: Epoxide as a precursor to secondary organic aerosol formation from isoprene photooxidation in the presence of nitrogen oxides, Proc. Natl. Acad. Sci., 110, 6718-6723, 2013b.

Lin, Y. H., Zhang, Z. F., Docherty, K. S., Zhang, H. F., Budisulistiorini, S. H., Rubitschun, C. L., Shaw, S. L., Knipping, E. M., Edgerton, E. S., Kleindienst, T. E., Gold, A., and Surratt, J. D.: Isoprene Epoxydiols as Precursors to Secondary Organic Aerosol Formation: Acid-Catalyzed Reactive Uptake Studies with Authentic Compounds, Environ. Sci. Technol., 46, 250-258, 10.1021/es202554c, 2012.

Ling, Y., Wang, Y., Duan, J., Xie, X., Liu, Y., Peng, Y., Qiao, L., Cheng, T., Lou, S., Wang, H., Li, X., and Xing, X.: Long-term aerosol size distributions and the potential role of volatile organic compounds (VOCs) in new particle formation events in Shanghai, Atmos. Environ., 202, 345-356, 10.1016/j.atmosenv.2019.01.018, 2019a.

Ling, Z., He, Z., Wang, Z., Shao, M., and Wang, X.: Sources of methacrolein and methyl vinyl ketone and their contributions to methylglyoxal and formaldehyde at a receptor site in Pearl River Delta, J. Environ. Sci., 79, 1-10, https://doi.org/10.1016/j.jes.2018.12.001, 2019b.

Liu, P., Ding, X., Bryant, D. J., Zhang, Y.-Q., Wang, J.-Q., Yang, K., Cheng, Q., Jiang, H., Wang, Z.-R., He, Y.-F., Li, B.-X., Zhao, M.-Y., Hamilton, J. F., Rickard, A. R., and Wang, X.-M.: Comparison of Isoprene-Derived Secondary Organic Aerosol Formation Pathways at an Urban and a Forest Site, ACS Earth Space Chem., 9, 1752-1767, 10.1021/acsearthspacechem.4c00398, 2025.

Liu, Y., Yang, X., Tan, J., and Li, M.: Concentration prediction and spatial origin analysis of criteria air pollutants in Shanghai, Environ. Pollut., 327, 121535, https://doi.org/10.1016/j.envpol.2023.121535, 2023a.

Liu, Y., Geng, G., Cheng, J., Liu, Y., Xiao, Q., Liu, L., Shi, Q., Tong, D., He, K., and Zhang, Q.: Drivers of Increasing Ozone during the Two Phases of Clean Air Actions in China 2013-2020, Environ. Sci. Technol., 57, 10.1021/acs.est.3c00054, 2023b.

McNeill, V. F., Woo, J. L., Kim, D. D., Schwier, A. N., Wannell, N. J., Sumner, A. J., and Barakat, J. M.: Aqueous-phase secondary organic aerosol and organosulfate formation in atmospheric aerosols: a modeling study, Environ. Sci. Technol., 46 15, 8075-8081, 2012.

Nguyen, T. B., Bates, K. H., Crounse, J. D., Schwantes, R. H., Zhang, X., Kjaergaard, H. G., Surratt, J. D., Lin, P., Laskin, A., Seinfeld, J. H., and Wennberg, P. O.: Mechanism of the hydroxyl radical oxidation of methacryloyl peroxynitrate (MPAN) and its pathway toward secondary organic aerosol formation in the atmosphere, Phys. Chem. Chem. Phys.,PCCP, 17, 17914-17926, 10.1039/c5cp02001h, 2015.

Orlando, J. J., Tyndall, G. S., and Paulson, S. E.: Mechanism of the OH-initiated oxidation of methacrolein, Geophys. Res. Lett, 26, 2191-2194, https://doi.org/10.1029/1999GL900453, 1999.

Park, C., Schade, G. W., and Boedeker, I.: Characteristics of the flux of isoprene and its oxidation products in an urban area, J. Geophys. Res.-atmosAtmos., 116, 10.1029/2011jd015856, 2011.

Paulot, F., Crounse, J. D., Kjaergaard, H. G., Kurten, A., St Clair, J. M., Seinfeld, J. H., and Wennberg, P. O.: Unexpected Epoxide Formation in the Gas-Phase Photooxidation of Isoprene, Science, 325, 730-733, 10.1126/science.1172910, 2009.

Piletic, I. R., Edney, E. O., and Bartolotti, L. J.: A computational study of acid catalyzed aerosol reactions of atmospherically relevant epoxides, Phys. Chem. Chem. Phys., 15, 18065-18076, 10.1039/c3cp52851k, 2013.

Pye, H. O. T., Pinder, R. W., Piletic, I. R., Xie, Y., Capps, S. L., Lin, Y.-H., Surratt, J. D., Zhang, Z., Gold, A., Luecken, D. J., Hutzell, W. T., Jaoui, M., Offenberg, J. H., Kleindienst, T. E., Lewandowski, M., and Edney, E. O.: Epoxide Pathways Improve Model Predictions of Isoprene Markers and Reveal Key Role of Acidity in Aerosol Formation, Environ. Sci. Technol., 47, 11056-11064, 10.1021/es402106h, 2013.

Pye, H. O. T., Murphy, B. N., Xu, L., Ng, N. L., Carlton, A. G., Guo, H., Weber, R., Vasilakos, P., Appel, K. W., Budisulistiorini, S. H., Surratt, J. D., Nenes, A., Hu, W., Jimenez, J. L., Isaacman-VanWertz, G.,

Misztal, P. K., and Goldstein, A. H.: On the implications of aerosol liquid water and phase separation for organic aerosol mass, Atmos. Chem. Phys., 17, 343-369, 10.5194/acp-17-343-2017, 2017.

Qin, M., Wang, X., Hu, Y., Ding, X., Song, Y., Li, M., Vasilakos, P., Nenes, A., and Russell, A. G.: Simulating Biogenic Secondary Organic Aerosol During Summertime in China, J. Geophys. Res. atmosAtmos., 123, 11,100-111,119, https://doi.org/10.1029/2018JD029185, 2018.

Rattanavaraha, W., Chu, K., Budisulistiorini, S. H., Riva, M., Lin, Y. H., Edgerton, E. S., Baumann, K., Shaw, S. L., Guo, H., King, L., Weber, R. J., Neff, M. E., Stone, E. A., Offenberg, J. H., Zhang, Z., Gold, A., and Surratt, J. D.: Assessing the impact of anthropogenic pollution on isoprene-derived secondary organic aerosol formation in PM2.5 collected from the Birmingham, Alabama, ground site during the 2013 Southern Oxidant and Aerosol Study, Atmos. Chem. Phys., 16, 4897-4914, 10.5194/acp-16-4897-2016, 2016.

Riedel, T. P., Lin, Y. H., Zhang, Z., Chu, K., Thornton, J. A., Vizuete, W., Gold, A., and Surratt, J. D.: Constraining condensed-phase formation kinetics of secondary organic aerosol components from isoprene epoxydiols, Atmos. Chem. Phys., 16, 1245-1254, 10.5194/acp-16-1245-2016, 2016.

Riedel, T. P., Lin, Y.-H., Budisulistiorini, H., Gaston, C. J., Thornton, J. A., Zhang, Z., Vizuete, W., Gold, A., and Surrattt, J. D.: Heterogeneous Reactions of Isoprene-Derived Epoxides: Reaction Probabilities and Molar Secondary Organic Aerosol Yield Estimates, Environ. Sci. Technol. Lett., 2, 38-42, 10.1021/ez500406f, 2015.

Schwantes, R. H., Teng, A. P., Nguyen, T. B., Coggon, M. M., Crounse, J. D., St. Clair, J. M., Zhang, X., Schilling, K. A., Seinfeld, J. H., and Wennberg, P. O.: Isoprene NO_3 Oxidation Products from the RO_2 + HO_2 Pathway, J. Phys. Chem. A, 119, 10158-10171, 10.1021/acs.jpca.5b06355, 2015.

Shrivastava, M., Andreae, M. O., Artaxo, P., Barbosa, H. M. J., Berg, L. K., Brito, J., Ching, J., Easter, R. C., Fan, J., Fast, J. D., Feng, Z., Fuentes, J. D., Glasius, M., Goldstein, A. H., Alves, E. G., Gomes, H., Gu, D., Guenther, A., Jathar, S. H., Kim, S., Liu, Y., Lou, S., Martin, S. T., McNeill, V. F., Medeiros, A., de Sa, S. S., Shilling, J. E., Springston, S. R., Souza, R. A. F., Thornton, J. A., Isaacman-VanWertz, G., Yee, L. D., Ynoue, R., Zaveri, R. A., Zelenyuk, A., and Zhao, C.: Urban pollution greatly enhances formation of natural aerosols over the Amazon rainforest, Nat. Commun., 10, 10.1038/s41467-019-08909-4, 2019.

Song, S., Gao, M., Xu, W., Shao, J., Shi, G., Wang, S., Wang, Y., Sun, Y., and McElroy, M. B.: Fine-particle pH for Beijing winter haze as inferred from different thermodynamic equilibrium models, Atmos. Chem. Phys., 18, 7423-7438, 10.5194/acp-18-7423-2018, 2018.

St. Clair, J. M., Rivera-Rios, J. C., Crounse, J. D., Knap, H. C., Bates, K. H., Teng, A. P., Jørgensen, S., Kjaergaard, H. G., Keutsch, F. N., and Wennberg, P. O.: Kinetics and Products of the Reaction of the First-Generation Isoprene Hydroxy Hydroperoxide (ISOPOOH) with OH, J. Phys. Chem. A, 120, 1441-1451, 10.1021/acs.jpca.5b06532, 2016.

Stone, E. A., Nguyen, T. T., Pradhan, B. B., and Man Dangol, P.: Assessment of biogenic secondary organic aerosol in the Himalayas, Environ. Chem. , 9, 263-272, https://doi.org/10.1071/EN12002, 2012.

Surratt, J. D., Chan, A., Eddingsaas, N. C., Chan, M. N., Loza, C. L., Kwan, A. J., Hersey, S. P., Flagan, R. C., Wennberg, P. O., and Seinfeld, J. H.: Reactive intermediates revealed in secondary organic aerosol formation from isoprene, Proc. Natl. Acad. Sci. U.S.A., 107, 6640-6645, 2010.

Surratt, J. D., Kroll, J. H., Kleindienst, T. E., Edney, E. O., Claeys, M., Sorooshian, A., Ng, N. L., Offenberg, J. H., Lewandowski, M., Jaoui, M., Flagan, R. C., and Seinfeld, J. H.: Evidence for organosulfates in secondary organic aerosol, Environ. Sci. Technol., 41, 517-527, 10.1021/es062081q, 2007.

Tao, S., Lu, X., Levac, N., Bateman, A. P., Nguyen, T. B., Bones, D. L., Nizkorodov, S. A., Laskin, J., Laskin, A., and Yang, X.: Molecular Characterization of Organosulfates in Organic Aerosols from Shanghai and Los Angeles Urban Areas by Nanospray-Desorption Electrospray Ionization High-Resolution Mass Spectrometry, Environ. Sci. Technol., 48, 10993-11001, 10.1021/es5024674, 2014.

Teng, A. P., Crounse, J. D., and Wennberg, P. O.: Isoprene Peroxy Radical Dynamics, J. Am. Chem. Soc, 139, 5367-5377, 10.1021/jacs.6b12838, 2017.

Wang, H., Wang, H., Lu, X., Lu, K., Zhang, L., Tham, Y. J., Shi, Z., Aikin, K., Fan, S., Brown, S. S., and Zhang, Y.: Increased night-time oxidation over China despite widespread decrease across the globe, Nat. Geosci, 16, 217-223, 10.1038/s41561-022-01122-x, 2023a.

Wang, M., Duan, Y., Xu, W., Wang, Q., Zhang, Z., Yuan, Q., Li, X., Han, S., Tong, H., Huo, J., Chen, J., Gao, S., Wu, Z., Cui, L., Huang, Y., Xiu, G., Cao, J., Fu, Q., and Lee, S.: Measurement report: Characterisation and sources of the secondary organic carbon in a Chinese megacity over 5 years from 2016 to 2020, Atmos. Chem. Phys., 22, 12789-12802, 10.5194/acp-22-12789-2022, 2022.

Wang, W., Wu, M. H., Li, L., Zhang, T., Liu, X. D., Feng, J. L., Li, H. J., Wang, Y. J., Sheng, G. Y., Claeys, M., and Fu, J. M.: Polar organic tracers in PM$_{2.5}$ aerosols from forests in eastern China, Atmos. Chem. Phys., 8, 7507-7518, 10.5194/acp-8-7507-2008, 2008.

Wang, Y., Zhao, Y., Wang, Y., Yu, J.-Z., Shao, J., Liu, P., Zhu, W., Cheng, Z., Li, Z., Yan, N., and Xiao, H.: Organosulfates in atmospheric aerosols in Shanghai, China: seasonal and interannual variability, origin, and formation mechanisms, Atmos. Chem. Phys., 21, 2959-2980, 10.5194/acp-21-2959-2021, 2021.

Wang, Y., Zhang, Y., Li, W., Wu, G., Qi, Y., Li, S., Zhu, W., Yu, J. Z., Yu, X., Zhang, H.-H., Sun, J., Wang, W., Sheng, L., Yao, X., Gao, H., Huang, C., Ma, Y., and Zhou, Y.: Important Roles and Formation of Atmospheric Organosulfates in Marine Organic Aerosols: Influence of Phytoplankton Emissions and Anthropogenic Pollutants, Environ. Sci. Technol., 57, 10284-10294, 10.1021/acs.est.3c01422, 2023b.

Wiedinmyer, C., Kimura, Y., McDonald-Buller, E. C., Emmons, L. K., Buchholz, R. R., Tang, W., Seto, K., Joseph, M. B., Barsanti, K. C., Carlton, A. G., and Yokelson, R.: The Fire Inventory from NCAR version 2.5: an updated global fire emissions model for climate and chemistry applications, Geosci. Model Dev., 16, 3873-3891, 10.5194/gmd-16-3873-2023, 2023.

Worton, D. R., Surratt, J. D., LaFranchi, B. W., Chan, A. W. H., Zhao, Y., Weber, R. J., Park, J.-H., Gilman, J. B., de Gouw, J., Park, C., Schade, G., Beaver, M., St Clair, J. M., Crounse, J., Wennberg, P., Wolfe, G. M., Harrold, S., Thornton, J. A., Farmer, D. K., Docherty, K. S., Cubison, M. J., Jimenez, J.-L., Frossard, A. A., Russell, L. M., Kristensen, K., Glasius, M., Mao, J., Ren, X., Brune, W., Browne, E. C., Pusede, S. E., Cohen, R. C., Seinfeld, J. H., and Goldsteint, A. H.: Observational Insights into Aerosol Formation from Isoprene, Environ. Sci. Technol., 47, 11403-11413, 10.1021/es4011064, 2013.

Xu, L., Middlebrook, A. M., Liao, J., de Gouw, J. A., Guo, H., Weber, R. J., Nenes, A., Lopez-Hilfiker, F. D., Lee, B. H., Thornton, J. A., Brock, C. A., Neuman, J. A., Nowak, J. B., Pollack, I. B., Welti, A., Graus, M., Warneke, C., and Ng, N. L.: Enhanced formation of isoprene-derived organic aerosol in sulfur-rich power plant plumes during Southeast Nexus, J. Geophys. Res. atmos Atmos., 121, 11,137-111,153, https://doi.org/10.1002/2016JD025156, 2016.

Xu, L., Guo, H., Boyd, C. M., Klein, M., Bougiatioti, A., Cerully, K. M., Hite, J. R., Isaacman-VanWertz, G., Kreisberg, N. M., Knote, C., Olson, K., Koss, A., Goldstein, A. H., Hering, S. V., de Gouw, J., Baumann, K., Lee, S.-H., Nenes, A., Weber, R. J., and Ng, N. L.: Effects of anthropogenic emissions on aerosol formation from isoprene and monoterpenes in the southeastern United States, Proc. Natl. Acad. Sci., 112, 37-42, doi:10.1073/pnas.1417609112, 2015.

Yan, K., Wang, J., Peng, R., Yang, K., Chen, X., Yin, G., Dong, J., Weiss, M., Pu, J., and Myneni, R. B.: HiQ-LAI: a high-quality reprocessed MODIS leaf area index dataset with better spatiotemporal consistency from 2000 to 2022, Earth Syst. Sci. Data, 16, 1601-1622, 10.5194/essd-16-1601-2024, 2024.

Yao, Y., Wang, W., Ma, K., Tan, H., Zhang, Y., Fang, F., and He, C.: Transmission paths and source areas of near-surface ozone pollution in the Yangtze River delta region, China from 2015 to 2021, J. Environ. Manage., 330, 117105, https://doi.org/10.1016/j.jenvman.2022.117105, 2023.

Ye, J., Abbatt, J. P. D., and Chan, A. W. H.: Novel pathway of SO$_2$ oxidation in the atmosphere: reactions with monoterpene ozonolysis intermediates and secondary organic aerosol, Atmos. Chem. Phys., 18, 5549-5565, 10.5194/acp-18-5549-2018, 2018.

Yee, L. D., Isaacman-VanWertz, G., Wernis, R. A., Kreisberg, N. M., Glasius, M., Riva, M., Surratt, J. D., de Sá, S. S., Martin, S. T., Alexander, M. L., Palm, B. B., Hu, W., Campuzano-Jost, P., Day, D. A., Jimenez, J. L., Liu, Y., Misztal, P. K., Artaxo, P., Viegas, J., Manzi, A., de Souza, R. A. F., Edgerton, E. S., Baumann, K., and Goldstein, A. H.: Natural and Anthropogenically Influenced Isoprene Oxidation in Southeastern United States and Central Amazon, Environ. Sci. Technol., 54, 5980-5991, 10.1021/acs.est.0c00805, 2020.

Zang, H., Zhao, Y., Huo, J., Zhao, Q., Fu, Q., Duan, Y., Shao, J., Huang, C., An, J., Xue, L., Li, Z., Li, C., and Xiao, H.: High atmospheric oxidation capacity drives wintertime nitrate pollution in the eastern Yangtze River Delta of China, Atmos. Chem. Phys., 22, 4355-4374, 10.5194/acp-22-4355-2022, 2022.

1084 Zhang, J., Liu, J., Ding, X., He, X., Zhang, T., Zheng, M., Choi, M., Isaacman-VanWertz, G., Yee, L., Zhang,
1085   H., Misztal, P., Goldstein, A. H., Guenther, A. B., Budisulistiorini, S. H., Surratt, J. D., Stone, E. A.,
1086   Shrivastava, M., Wu, D., Yu, J. Z., and Ying, Q.: New formation and fate of Isoprene SOA markers
1087   revealed by field data-constrained modeling, npj Clim. Atmos. Sci., 6, 69, 10.1038/s41612-023-00394-3,
1088   2023.

1089 Zhang, Y.-Q., Chen, D.-H., Ding, X., Li, J., Zhang, T., Wang, J.-Q., Cheng, Q., Jiang, H., Song, W., Ou, Y.-
1090   B., Ye, P.-L., Zhang, G., and Wang, X.-M.: Impact of anthropogenic emissions on biogenic secondary
1091   organic aerosol: observation in the Pearl River Delta, southern China, Atmos. Chem. Phys., 19, 14403-
1092   14415, 10.5194/acp-19-14403-2019, 2019.

1093 Zhang, Y.-Q., Ding, X., He, Q.-F., Wen, T.-X., Wang, J.-Q., Yang, K., Jiang, H., Cheng, Q., Liu, P., Wang,
1094   Z.-R., He, Y.-F., Hu, W.-W., Wang, Q.-Y., Xin, J.-Y., Wang, Y.-S., and Wang, X.-M.: Observational Insights
1095   into Isoprene Secondary Organic Aerosol Formation through the Epoxide Pathway at Three Urban Sites
1096   from Northern to Southern China, Environ. Sci. Technol., 10.1021/acs.est.1c06974, 2022.

1097 Zhao, D., Schmitt, S. H., Wang, M., Acir, I.-H., Tillmann, R., Tan, Z., Novelli, A., Fuchs, H., Pullinen, I.,
1098   Wegener, R., Rohrer, F., Wildt, J., Kiendler-Scharr, A., Wahner, A., and Mentel, T. F.: Effects of NOx and
1099   SO$_2$ on the secondary organic aerosol formation from photooxidation of α-pinene and limonene, Atmos.
1100   Chem. Phys., 18, 1611-1628, 10.5194/acp-18-1611-2018, 2018.

1101 Zhao, Z., Xu, Q., Yang, X., and Zhang, H.: Heterogeneous Ozonolysis of Endocyclic Unsaturated Organic
1102   Aerosol Proxies: Implications for Criegee Intermediate Dynamics and Later-Generation Reactions, ACS
1103   Earth Space Chem., 3, 344-356, 10.1021/acsearthspacechem.8b00177, 2019.

1104 Zheng, B., Tong, D., Li, M., Liu, F., Hong, C., Geng, G., Li, H., Li, X., Peng, L., Qi, J., Yan, L., Zhang, Y.,
1105   Zhao, H., Zheng, Y., He, K., and Zhang, Q.: Trends in China's anthropogenic emissions since 2010 as the
1106   consequence of clean air actions, Atmos. Chem. Phys., 18, 14095-14111, 10.5194/acp-18-14095-2018,
1107   2018.

1108 Zhong, Y., Chen, J., Zhao, Q., Zhang, N., Feng, J., and Fu, Q.: Temporal trends of the concentration and
1109   sources of secondary organic aerosols in PM$_{2.5}$ in Shanghai during 2012 and 2018, Atmos. Environ., 261,
1110   118596, https://doi.org/10.1016/j.atmosenv.2021.118596, 2021.

1111 Zhou, M., Zheng, G., Wang, H., Qiao, L., Zhu, S., Huang, D., An, J., Lou, S., Tao, S., Wang, Q., Yan, R.,
1112   Ma, Y., Chen, C., Cheng, Y., Su, H., and Huang, C.: Long-term trends and drivers of aerosol pH in eastern
1113   China, Atmos. Chem. Phys., 22, 13833-13844, 10.5194/acp-22-13833-2022, 2022.

1114